

A Comprehensive study of open clusters Czernik 14, Haffner 14, Haffner 17 and King 10 using multicolour photometry and Gaia DR2 astrometry

D. Bisht^{1,*}, Qingfeng Zhu¹, R. K. S. Yadav², Alok Durgapal³, and Geeta Rangwal³

¹ *Key Laboratory for Researches in Galaxies and Cosmology, University of Science and Technology of China, Chinese Academy of Sciences, Hefei, Anhui, 230026, China*

² *Aryabhata Research Institute of Observational Sciences, Manora Peak, Nainital 263129, India*

³ *Department of physics, DSB campus, KU Nainital, India*

1 February 2022

ABSTRACT

This paper presents an investigation on the four open clusters Czernik 14, Haffner 14, Haffner 17 and King 10 located near the Perseus arm of Milky Way Galaxy using **Gaia DR2**, **2MASS**, **WISE**, **APASS** and **Pan-STARRS1** data sets. We find normal interstellar extinction in twelve photometric bands for these clusters. Likely cluster members are identified as 225, 353, 350 and 395 for Czernik 14, Haffner 14, Haffner 17 and King 10, respectively by using Gaia DR2 proper motion data. Radii are determined as 3.5, 3.7, 6.2 and 5.7 arcmin for Czernik 14, Haffner 14, Haffner 17 and King 10 respectively. Mean proper motions in RA and DEC are estimated as $(-0.42 \pm 0.02, -0.38 \pm 0.01)$, $(-1.82 \pm 0.009, 1.73 \pm 0.008)$, $(-1.17 \pm 0.007, 1.88 \pm 0.006)$ and $(-2.75 \pm 0.008, -2.04 \pm 0.006)$ mas yr⁻¹ for Czernik 14, Haffner 14, Haffner 17 and King 10, respectively. The comparison of observed CMDs with solar metallicity isochrones leads to an age of 570 ± 60 , 320 ± 35 , 90 ± 10 and 45 ± 5 Myr for these clusters. The distances 2.9 ± 0.1 , 4.8 ± 0.4 , 3.6 ± 0.1 and 3.8 ± 0.1 kpc determined using parallax are comparable with the values derived by the isochrone fitting method. Mass function slopes are found to be in good agreement with the Salpeter value. The total masses are derived as 348, 595, 763 and 1088 M_{\odot} for the clusters Czernik 14, Haffner 14, Haffner 17 and King 10, respectively. Evidence for the existence of mass-segregation effect is observed in each cluster. Using the Galactic potential model, Galactic orbits are derived for the clusters. The present study indicates that all clusters under study follow a circular path around the Galactic center.

Key words: Star:-Colour-Magnitude diagrams - open cluster and associations: individual (Czernik 14, Haffner 14, Haffner 17, King 10)-astrometry-Dynamics-Galactic orbits

1 INTRODUCTION

Open clusters (OCs) are convenient probes in studying the structure and evolution of the Milky Way Galaxy. Since OCs are formed by the collapse and fragmentation of huge molecular cloud (e.g. Harris & Pudritz 1994; Bate et al. 2003), they become ready samples to study the stellar evolution history. The second Gaia data release (Gaia DR2) provides

accurate five parameter astrometric data (Positions, proper motions and parallaxes) for more than 1.3 billion sources. Gaia DR2 is very effective and it will be a showcase of how effectively these data can be used to identify cluster members, especially in the crowded regions. Open clusters have been the subject of many studies over the past decades. They are very important and widely used to distinguish the Galactic disk properties, such as understanding the spiral arms of the Milky Way (e.g. Bonatto et al. 2006; van den Bergh 2006), the stellar metallicity gradient (Janes 1979; Geisler et al. 1997; Frinchaboy et al. 2013) and the age-metallicity relationship in the Galactic disk (e.g. Carraro & Chiosi 1994;

* E-mail: dbisht@ustc.edu.cn; zhuqf@ustc.edu.cn;
rkant@aries.res.in; alokdurgapal@gmail.com; geetarangwal91@gmail.com

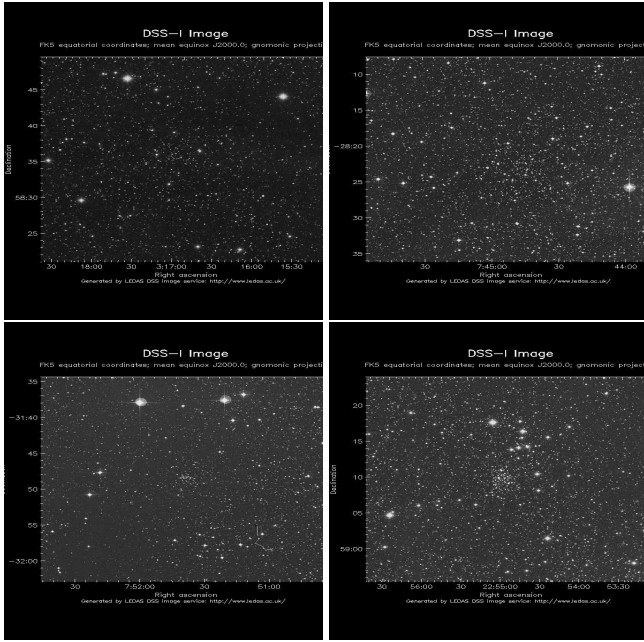


Figure 1. Identification maps of clusters Czernik 14 (Top left), Haffner 14 (Top right), Haffner 17 (Bottom Left) and King 10 (Bottom right) taken from LEDAS.

Carraro et al. 1998; Salaris et al. 2004; Margrini et al. 2009). Young open clusters are essential laboratories to understand about star formation scenario. The intermediate age clusters are very useful in testing stellar isochrones and dynamical evolution of cluster stars. Over the last decade, the clusters inspection rate has been lifted exceptionally well. This can be attributed to the appearance of multiple wide-ranging Near-Infrared (NIR) and Mid-Infrared (MIR) surveys, such as GLIMPSE, 2MASS (Skrutskie et al. 2006), UKIDSS-GPS (Lucas et al. 2008), VISTA-VVV (Minniti et al. 2010) and *WISE* (Wright et al. 2010).

The most impressive cause to employ 2MASS, WISE and Gaia DR2 database is that they deliver us a robust tool to recognize star clusters behind the broad hydrogen clouds. The 2MASS survey has been manifest to be a strong tool in the investigation of the framework and stellar content of open clusters (Bonatto & Bica 2003). Lately, many OCs have been discovered by exploring 2MASS data (Kronberger et al. 2006; Froebrich et al. (2007); Koposov et al. (2008); Glushkova et al. (2010)). It is expected that the Gaia mission will fully transform our knowledge of the structure and dynamics of the Galaxy (Gaia Collaboration et al. 2016a). The latest version of the Gaia data (Gaia DR2) covers more than 1.3 billion sources and was made public on 2018 April 24 (Gaia Collaboration et al. 2016a,b). Gaia DR2 catalogue contains three photometric bands (G, G_{BP}, G_{RP}), the precise astrometry at the sub-milliarcsecond level and parallax (Gaia collaboration et al., 2018b).

The OCs mass function gives direction about the star formation process. Phenomenal works have been done on the mass function of OCs during the last two decades (e.g. Baume et al. 2004, Durgapal and Pandey 2001, Pandey et al. 2001, Phelps and Janes 1993, Piatti et al. 2002, Piskunov et al. 2004, Sagar and Griffiths 1998, Prisinzano et al. 2001,

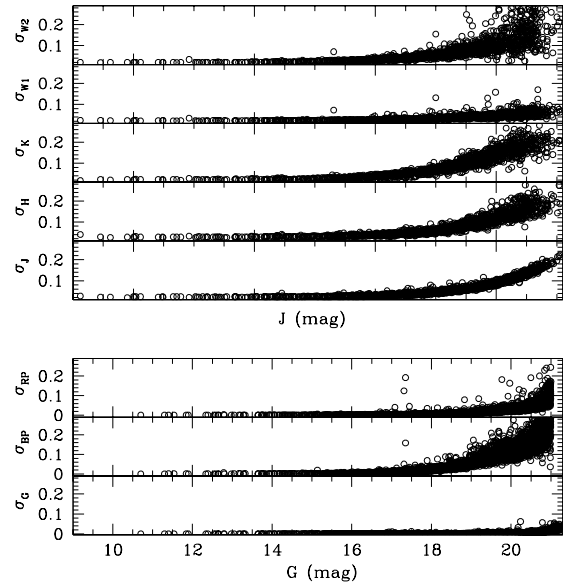


Figure 2. Photometric errors in Gaia passbands G , G_{BP} and G_{RP} against G magnitude in three lower panels while photometric errors in J , H , K , W_1 and W_2 magnitudes against J magnitude in upper five panels.

Scalo 1986, Scalo et al. 1998, Sung and Bessell 2004, Yadav and Sagar 2002, 2004a, Bisht et al. 2017 & 2019 and Geeta et al. 2019). Despite all these remarkable works, the universality of initial mass functions is still a question of debate (Elmegreen 2000, Larson and Nakamoto 1999). Additionally, the mass segregation evaluation in OCs gives proof about the spatial arrangement of massive and faint stars within the area of the cluster.

In the present study, we also focus on the study of Galactic orbits of these open star clusters. Orbits carry information about the history of path of the cluster. Orbits are given by the environment in which the cluster lives under the Galactic gravitational potential of the Milky Way. Hence the orbits bring information about the clusters themselves, as well as about the Milky Way.

In this paper, we attempt to investigate the members, distances and mean proper motion of open clusters Czernik 14, Haffner 14, Haffner 17 and King 10 using the high precision astrometry and photometry taken from the Gaia DR2 catalogue. The main goal of this article is to study the fundamental parameters (age, distance, reddening, etc.) of the clusters, luminosity functions (LFs), mass functions (MFs) and Galactic orbits of the target objects. We did not find a detailed study of these clusters in the literature. Available information for these clusters is given below.

Czernik 14: This cluster is positioned at $\alpha = 3^h 16^m 54^s$ and $\delta = 58^\circ 36' 0''$ (J2000.0), corresponding to Galactic coordinates $l = 140^\circ.92$ and $b = 0^\circ.9$. It is part of the Perseus arm in the second Galactic quadrant.

Haffner 14: The location of this cluster is at $\alpha = 7^h 44^m 51^s$ and $\delta = -28^\circ 22' 0''$ (J2000.0), corresponding to Galactic coordinates $l = 243^\circ.98$ and $b = -2^\circ.1$. This is close to Perseus arm in the third Galactic quadrant of the Milky Way.

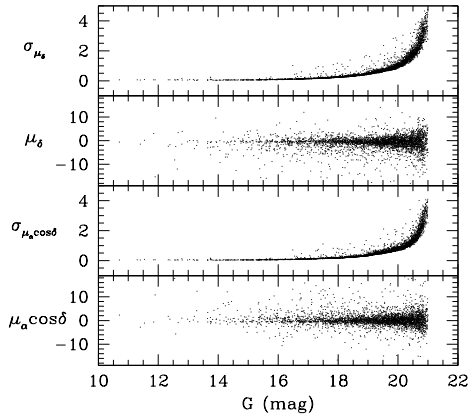


Figure 3. Plot of Proper motions and their errors versus G magnitude for the cluster Czernik 14 is shown as an example.

Haffner 17: This is positioned at $\alpha = 7^h 51^m 37^s$ and $\delta = -31^\circ 49' 0''$ (J2000.0), corresponding to the galactic coordinates $l = 247^\circ.71$ and $b = -2^\circ.5$. As Haffner 14, it is also near to Perseus arm in the third Galactic quadrant. Pedreros (2000) has estimated basic parameters of this cluster using UBV data. The interstellar reddening, distance modulus and cluster age was estimated as 1.26 ± 0.04 , 12.3 ± 0.2 mag and 50 Myr.

King 10: This is located at $\alpha = 22^h 54^m 54^s$ and $\delta = 59^\circ 10' 0''$ (J2000.0), corresponding to Galactic coordinates $l = 108^\circ.48$ and $b = -0^\circ.4$. CCD $UBVRI$ photometric analysis is performed by Mohan et al. (1992). They found a variable reddening in the cluster with distance and age as 3.2 Kpc and ≤ 50 Myr. It is a part of the Perseus arm in the second Galactic quadrant.

This paper is organized as follows. Section 2 presents the different data sets used in this study. Section 3 describes the method for members selection. In section 4, we derive different fundamental parameters of the clusters. Section 5 is devoted to the luminosity and mass function of the clusters. The dynamical state of the clusters is described in section 6. In section 7, orbits of the clusters are calculated. Finally, the conclusion of the present study is given in the last section.

2 DATA USED

We collected astrometric and photometric data from Gaia DR2 along with broad-band photometric data from APASS, Pan-STARRS1, 2MASS and WISE for clusters Czernik 14, Haffner 14, Haffner 17 and King 10. We cross-matched each catalog for the present analysis. The descriptions of used data set are the following:

2.1 The multi-dimensional Gaia DR2 data set

We used Gaia DR2 (Gaia Collaboration et al. 2018a) data for the astrometric analysis of the clusters. Gaia data consist of five parametric astrometric solution-positions on the sky (α, δ), parallaxes and ($\mu_\alpha \cos \delta, \mu_\delta$) with a limiting magnitude of $G = 21$ mag. The completeness of the Gaia survey

has much improved now in comparison to the first data release. The Gaia DR2 is essentially complete between $G=12$ to 17 mag. The G band covers the whole optical wavelength ranging from 330 to 1050 nm, while G_{BP} and G_{RP} bands cover the wavelength range 330-680 nm and 630-1050 nm, respectively (Evans et al. 2018). The central wavelengths are 673, 532, 797 nm for G , G_{BP} and G_{RP} bands respectively (Jordi et al. 2010). Parallax uncertainties are in the range of ~ 0.04 milliarcsecond (mas) for sources at $G \leq 14$ mag, ~ 0.1 mas for sources with $G \sim 17$ mag, and 0.7 mas at $G=20$ mag (Lindgren et al. 2018). The uncertainties in the respective proper motion components are up to 0.06 mas yr^{-1} (for $G \leq 15$ mag), 0.2 mas yr^{-1} (for $G \sim 17$ mag) and 1.2 mas yr^{-1} (for $G \sim 20$ mag). The proper motion and their corresponding errors are plotted against G magnitude in Fig 3. In this figure, errors in proper motion components are ~ 1.2 at $G \sim 20$ mag.

2.2 2MASS data

The 2MASS (Skrutskie et al. 2006) used two highly automated 1.3m telescopes (one at Mt. Hopkins, Arizona (AZ), USA and other at the Cerro Tololo Inter-American Observatory, Chile) with a 3-channel camera, each having a (256×256) array of HgCdTe detectors. This 2MASS photometric catalogue provides J ($1.25 \mu\text{m}$), H ($1.65 \mu\text{m}$) and K_s ($2.17 \mu\text{m}$) band photometry for millions of galaxies and nearly a half-billion stars (Carpenter, 2001). The sensitivity of the 2MASS catalogue is 15.8 mag for J , 15.1 mag for H and 14.3 mag for K_s band at a signal-to-noise of 10. *VizieR*¹ was used to extract J , H and K_s photometric data in circular areas centered on the clusters under study. Identification maps for the clusters are taken from Leicester Database and Archive Service (LEDAS) and shown in Fig 1.

The stars with observational uncertainties ≥ 0.20 mag are excluded, and photometric completeness limit is applied on the 2MASS data to avoid the over-sampling at the lower parts in the cluster's colour-magnitude diagrams (Bonatto et al. 2004). The errors given in 2MASS catalogue for J , H and K_s band are plotted against J magnitudes in Fig 2. This figure shows the mean error in J , H and K_s band is ≤ 0.05 at $J \sim 13.0$ mag. The errors become ~ 0.09 at $J \sim 15$ mag.

2.3 WISE data

The WISE database is a NASA Medium Class Explorer mission that conducted a digital imaging survey of the entire sky in the mid-IR bands. The effective wavelength of mid-IR bands are $3.35 \mu\text{m}$ (W1), $4.60 \mu\text{m}$ (W2), $11.56 \mu\text{m}$ (W3) and $22.09 \mu\text{m}$ (W4) (Wright et al. 2010). This data has been taken from ALLWISE source catalogue for the clusters under study. This catalogue has achieved 5σ point source sensitivities better than 0.08, 0.11, 1 and 6 mJy at 3.35, 4.60, 11.56 and $22.09 \mu\text{m}$, which is expected to be more than 99% of the sky. These sensitivities are 16.5, 15.5, 11.2 and 7.9 for W1, W2, W3 and W4 bands correspond to vega magnitudes.

¹ vizier.u-starsbg.fr/viz-bin/VizieR?-source=II/246

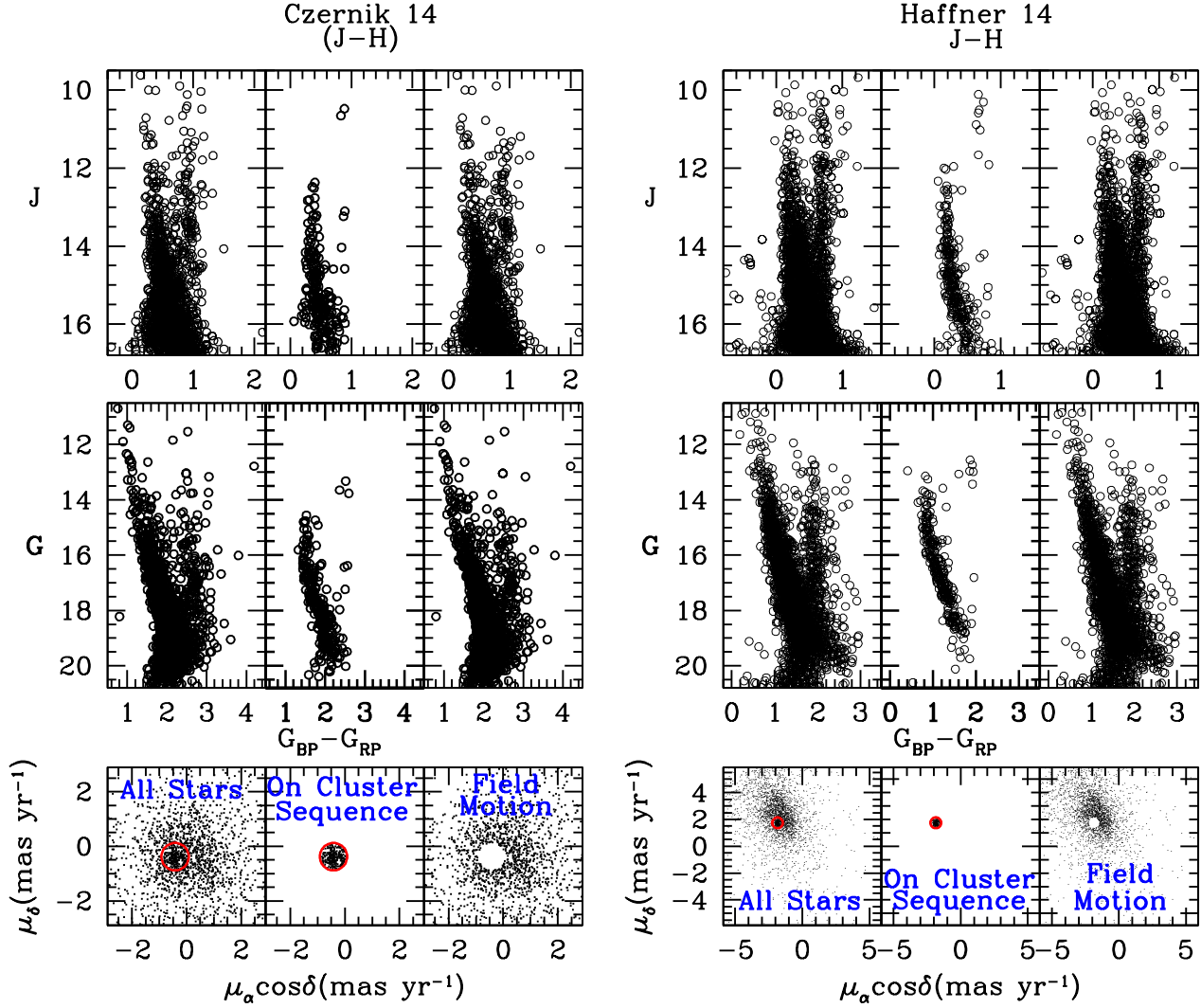


Figure 4. (Bottom panels) Proper-motion vector point diagrams (VPDs) for clusters Czernik 14 and Haffner 14. (Top panels) J versus $J - H$ colour magnitude diagrams. (Middle panels) G versus $(G_{BP} - G_{RP})$ colour magnitude diagrams. For each cluster CMDs, (Left panel) The entire sample. (Center) Stars within the circle of 0.5 and 0.4 mas yr^{-1} radius centered around the mean proper motion of Czernik 14 and Haffner 14 respectively. (Right) Probable background/foreground field stars in the direction of these clusters. All plots show only stars with PM error smaller than 1 mas yr^{-1} in each coordinate.

2.4 APASS data

The American Association of Variable Star Observers (AAVSO) Photometric All-Sky Survey (APASS) is organized in five filters: B , V (Landolt) and g' , r' , i' proving stars with V band magnitude range from 7 to 17 mag (Heden & Munari 2014). DR9 is the latest catalogue and covers about 99% sky (Heden et al. 2016). We have extracted this data from <http://vizier.u-strasbg.fr/viz-bin/VizieR?source=II/336>.

2.5 Pan-STARRS1 data

The Pan-STARRS1 survey (Hodapp et al. 2004) imaged the sky in five broad-band filters, g , r , i , z , y , covering from 400 nm to 1 μm (Stubbs et al. 2010). The mean 5σ point source limiting sensitivities in g , r , i , z , and y bands are

23.3, 23.2, 23.1, 22.3, and 21.4 mag, respectively (Chambers et al. 2016). The effective wavelengths of these filters are 481, 617, 752, 866, and 962 nm, respectively (Schlafly et al. 2012; Tonry et al. 2012). The photometric accuracy of this data has been demonstrated by Schlafly et al. (2012) and Magnier et al. (2013).

3 MEAN PROPER MOTION OF CLUSTERS AND MEMBER SELECTION

Field region stars always affect the accurate measurements of cluster fundamental parameters. Proper motion plays the most important role to separate non members from cluster's area. To select possible cluster members of Czernik 14, Haffner 14, Haffner 17 and King 10, we applied Gaia DR2 proper motion data and parallax data.

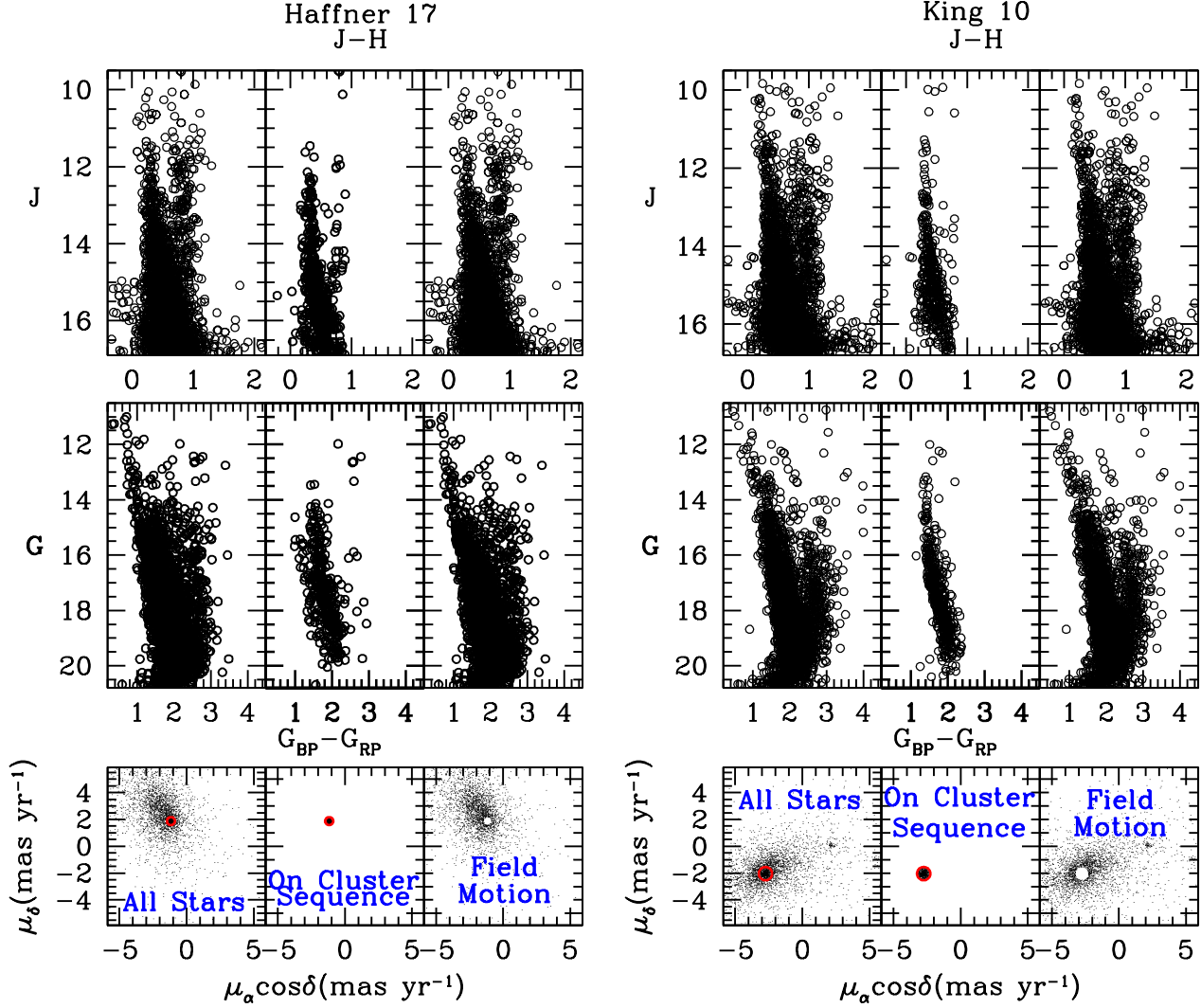


Figure 5. Same as Fig 4 for clusters Haffner 17 and King 10. Radii of the circles centered around the mean PM are 0.4 and 0.5 mas yr^{-1} as shown in the VPDs for Haffner 17 and King 10.

PMs, $\mu_\alpha \cos \delta$ and μ_δ are plotted as VPDs in the bottom panels of Fig 4 and Fig 5. The top row panels in each cluster show the corresponding J versus $(J - H)$ CMDs and G versus $(G_{BP} - G_{RP})$. The left panel in the CMDs shows all stars present in the cluster's area, while the middle and right panels show the probable cluster members and non member stars respectively. A circle of 0.5, 0.4, 0.4 and 0.5 mas yr^{-1} around the center of the member stars distribution in the VPDs characterize our membership criteria. The picked radius is an agreement between losing cluster members with poor PMs and the involvement of non member stars. The CMDs of the probable members are shown in the middle row panels in each clusters CMDs as shown in Fig 4 and Fig 5. The main sequence of the cluster is separated out. These stars have a PM error of $\leq 1 \text{ mas yr}^{-1}$.

For the precise estimation of mean proper motion, we deal with only probable cluster members based on clusters VPDs and CMDs as shown in Fig 6. By fitting the Gaussian function into the constructed histograms provides mean proper motion in the directions of RA and DEC, as shown

in Fig 6. To centered the Gaussian, we focused on the peak of the distribution. In this way, we found the mean-proper motion in RA and DEC directions as -0.42 ± 0.02 and $-0.38 \pm 0.01 \text{ mas yr}^{-1}$ for Czernik 14, -1.82 ± 0.009 and $1.73 \pm 0.008 \text{ mas yr}^{-1}$ for Haffner 14, -1.17 ± 0.007 and $1.88 \pm 0.006 \text{ mas yr}^{-1}$ for Haffner 17 and -2.75 ± 0.008 and $-2.04 \pm 0.006 \text{ mas yr}^{-1}$ for King 10. The estimated values of mean proper motions for each cluster is in fair agreement with the values given by Cantat-Gaudin (2018). Cantat-Gaudin catalogue (2018) reports the membership probabilities of these OCs. We have matched our probable members with this catalogue and selected stars having a probability higher than 40% for each cluster and used to derive fundamental parameters of the clusters.

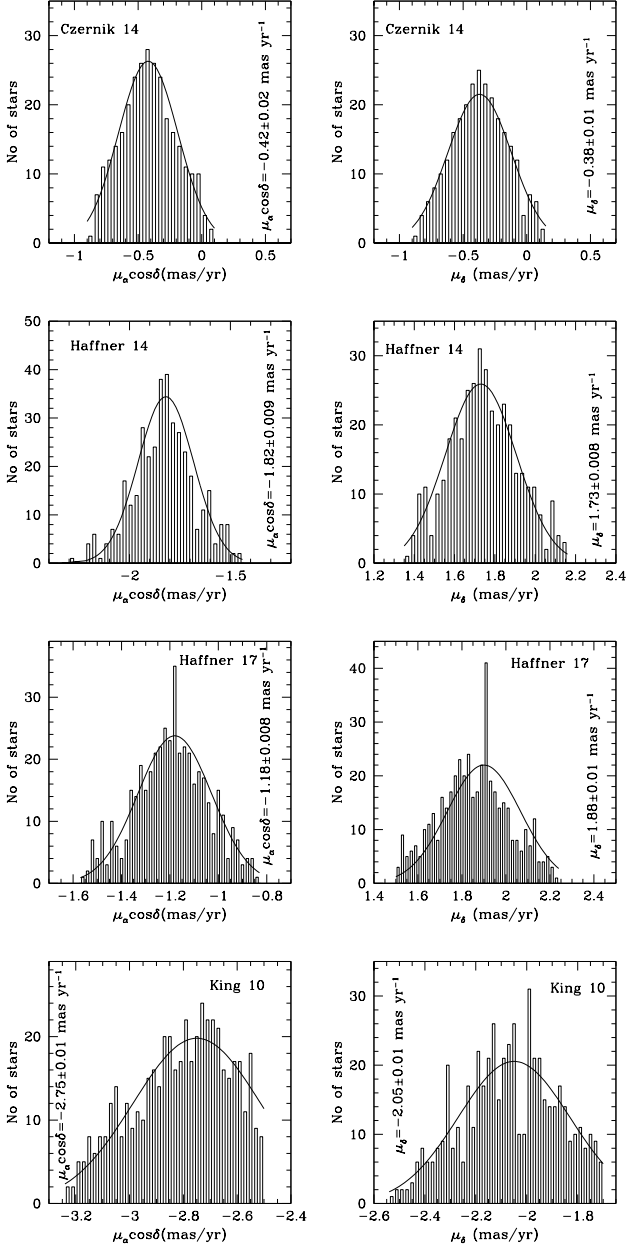


Figure 6. Proper motion histograms in 0.1 mas yr^{-1} bins in $\mu_\alpha \cos \delta$ and μ_δ of the clusters. The Gaussian function fit to the central bins provides the mean values in both directions as shown in each panel.

4 CLUSTERS STRUCTURE, EXTINCTION LAW AND FUNDAMENTAL PARAMETERS EVALUATION

4.1 Center estimation:

To understand cluster properties, the elementary step is to find clusters central coordinates. In the previous studies, the center has been determined just by the visual inspection (Becker & Fenkart 1971; Romanishim & Angel 1980). In this paper, we applied the star-count method using the stars selected from proper motion. The histograms are con-

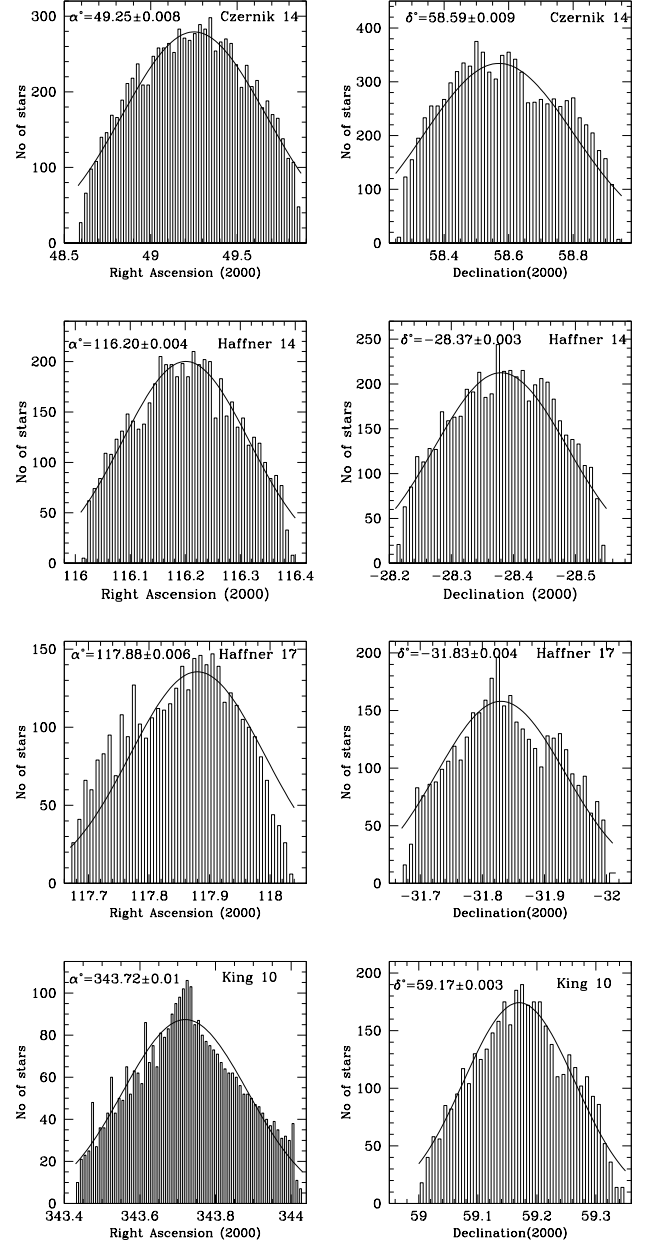


Figure 7. Profiles of stellar counts across clusters Czernik 14, Haffner 14, Haffner 17 and King 10 using Gaia DR2. The Gaussian fits have been applied. The center of symmetry about the peaks of Right Ascension and Declination is taken to be the position of the cluster's center.

structed for the clusters in RA and DEC directions by using bf most probable cluster members, selected in above section as shown in Fig 7. The Gaussian curve-fitting is performed to the star counts profiles in RA and DEC directions. Using this method, the coordinates of the center are found to be $\alpha^\circ = 49.25 \pm 0.008 \text{ deg}$ ($3^h 17^m 00^s$) and $\delta^\circ = 58.59 \pm 0.009 \text{ deg}$ ($58^\circ 35' 24''$) for Czernik 14, $\alpha^\circ = 116.20 \pm 0.004 \text{ deg}$ ($7^h 44^m 48^s$) and $\delta^\circ = -28.37 \pm 0.003 \text{ deg}$ ($-28^\circ 22' 12''$) for Haffner 14, $\alpha^\circ = 117.88 \pm 0.006 \text{ deg}$ ($7^h 51^m 31^s$) and $\delta^\circ = -31.83 \pm 0.004 \text{ deg}$ ($-31^\circ 49' 48''$) for Haffner 17 and

$\alpha^\circ = 343.72 \pm 0.01$ deg ($22^h 54^m 53^s$) and $\delta^\circ = 59.17 \pm 0.003$ deg ($59^\circ 10' 12''$) for King 10. These estimated values are in good agreement with the values given by Dias et al. (2002). Our derived values of the center of cluster are also matched well with Cantat-Gaudin (2018) catalogue within uncertainty.

4.2 Cluster radius and radial stellar surface density

Estimation of cluster radius is one of the most important fundamental properties. We construct a radial density profile (RDP) for open clusters Czernik 14, Haffner 14, Haffner 17 and King 10 using stars with $G \leq 19$ mag. We drew many concentric rings around the cluster center with an equal increment in radius. The number density, ρ_i , in the i^{th} zone is determined by using the formula of $\rho_i = \frac{N_i}{A_i}$, where N_i is the number of cluster stars and A_i is the area of the i^{th} zone. The radii of the clusters are calculated on the basis of the visual inspection of RDPs. The radii at which each distribution flattens are considered as cluster radius. The error in the background density level is shown with dotted lines in Fig 8. RDP becomes flat at $r \sim 3.5'$ ($\log(\text{radius})=0.54$), $3.7'$ ($\log(\text{radius})=0.57$), $6.2'$ ($\log(\text{radius})=0.79$) and $5.7'$ ($\log(\text{radius})=0.76$) for the clusters Czernik 14, Haffner 14, Haffner 17 and King 10. After this point, cluster stars merged with non-member stars, which is seen in Fig 8. Therefore, we considered $3.5'$, $3.7'$, $6.2'$ and $5.7'$ as the cluster radius. The observed radial density profile was fitted using King (1962) profile:

$$f(r) = f_b + \frac{f_0}{1+(r/r_c)^2}$$

where f_b , f_0 and r_c are background density, central star density and the core radius of the cluster respectively. The errors bar are calculated using the statistics Poisson error in each shell as $P_{err} = \frac{1}{\sqrt{N}}$. By fitting the King model to the cluster density profiles, we estimate the structural parameters of each cluster. Using Gaia DR2 photometry, the structural parameters for the clusters are obtained as, $f_b=4.27$ star/arcmin², $f_0=9.77$ star/arcmin² and $r_c=0.84$ arcmin for Czernik 14, $f_b=9.68$ star/arcmin², $f_0=18.89$ star/arcmin² and $r_c=0.86$ arcmin for Haffner 14, $f_b=5.90$ star/arcmin², $f_0=32.33$ star/arcmin² and $r_c=1.2$ arcmin for Haffner 17 and $f_b=5.57$ star/arcmin², $f_0=24.46$ star/arcmin² and $r_c=1.7$ arcmin for King 10.

Limiting radius (r_{lim}) of each cluster is calculated by comparing $f(r)$ to a background density level, f_b , defined as

$$f_b = f_{bg} + 3\sigma_{bg}$$

where σ_{bg} is uncertainty of f_{bg} . Therefore, r_{lim} is calculated according to the following formula (Bukowiecki et al. 2011)

$$r_{lim} = r_c \sqrt{\left(\frac{f_0}{3\sigma_{bg}} - 1\right)}$$

The value of limiting radius is found to be 4.5, 4.1, 6.8, and 6.2 arcmin for Czernik 14, Haffner 14, Haffner 17 and King 10, respectively. r_c and r_{lim} are used to deter-

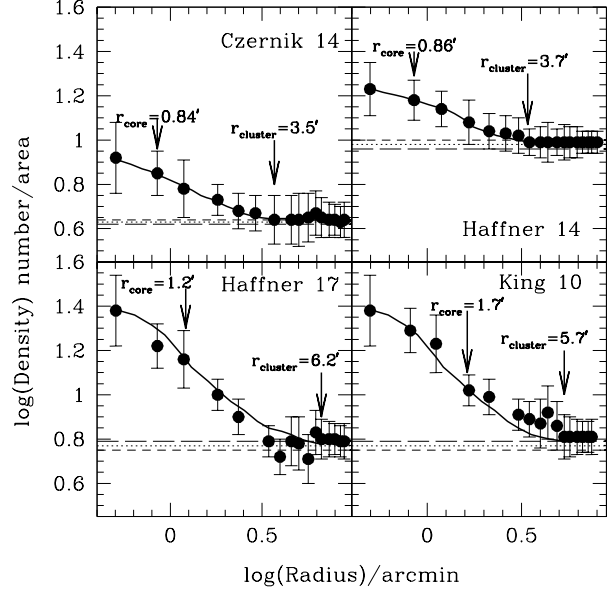


Figure 8. Surface density distribution of the clusters Czernik 14, Haffner 14, Haffner 17 and King 10 using Gaia DR2 G band data. Errors are determined from sampling statistics ($= \frac{1}{\sqrt{N}}$ where N is the number of cluster members used in the density estimation at that point). The smooth line represents the fitted profile of King (1962) whereas the dotted line shows the background density level. Long and short dash lines represent the errors in background density.

mine the value of concentration parameter $c = \log(\frac{r_{lim}}{r_c})$ (Peterson & King, 1975) as 0.73, 0.67, 0.75 and 0.56 for the clusters Czernik 14, Haffner 14, Haffner 17 and King 10, respectively. Maciejewski & Niedzielski (2007) suggested that r_{lim} may vary for particular clusters from $2r_c$ to $7r_c$. In this study, all clusters show a good agreement with Maciejewski & Niedzielski (2007).

The density contrast parameter ($\delta_c = 1 + \frac{f_0}{f_b}$) is calculated for all the clusters under study using member stars selected from proper motion data. Current evaluation of δ_c (3.3, 2.9, 6.3 and 5.4 for Czernik 14, Haffner 14, Haffner 17 and King 10, respectively) are lower than the values ($7 \leq \delta_c \leq 23$) given by Bonatto & Bica (2009). This estimation of δ_c indicates that all clusters are sparse.

The tidal radius of clusters are normally influenced by the effects of Galactic tidal fields and later internal relaxation and dynamical evolution of clusters (Allen & Martos 1988). The tidal radius is determined as follows.

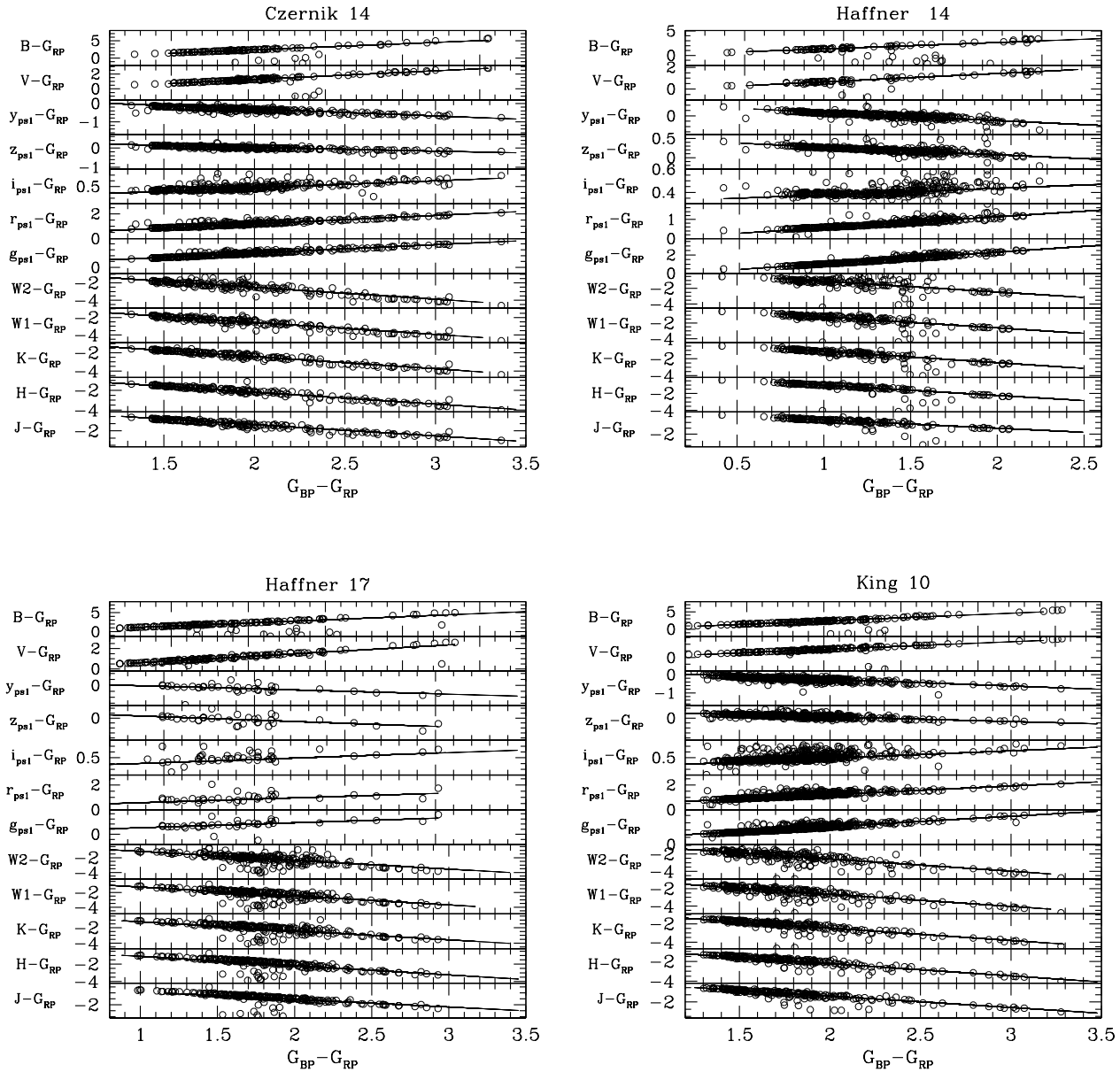
The Galactic mass M_G inside a Galactocentric radius R_G is given by (Genzel & Townes, 1987),

$$M_G = 2 \times 10^8 M_\odot \left(\frac{R_G}{30 \text{ pc}}\right)^{1.2}$$

Estimated values of Galactic mass inside the Galactocentric radius (see Sec. 4.5) are found as $2.2 \times 10^{11} M_\odot$, $2.8 \times 10^{11} M_\odot$, $2.5 \times 10^{11} M_\odot$ and $2.1 \times 10^{11} M_\odot$ for the clusters Czernik 14, Haffner 14, Haffner 17 and King 10 respectively. Present estimation of Galactic mass are close to the value ($2.9 \pm 0.4 \times 10^{11} M_\odot$) determined by Gibbons, Belokurov & Evans (2014) within 50 kpc radius of the Galaxy.

Table 1. Structural parameters of the clusters under study. Background and central density are in the unit of stars per arcmin². Core radius (r_c) and tidal radius (R_t) are in arcmin and pc.

Name	f_0	f_b	r_c	r_c	R_t	R_t	δ_c	r_{lim}	c
			arcmin	parsec	arcmin	parsec		arcmin	
Czernik 14	9.77	4.27	0.84	0.71	11.51 ± 0.49	9.71 ± 0.50	3.3	4.5	0.73
Haffner 14	18.89	9.68	0.86	1.20	9.21 ± 0.50	12.86 ± 0.70	2.9	4.1	0.67
Haffner 17	32.33	5.90	1.2	1.3	12.52 ± 0.57	13.11 ± 0.60	6.3	6.8	0.75
King 10	24.46	5.57	1.7	1.9	12.13 ± 0.45	13.41 ± 0.50	5.4	6.2	0.56

**Figure 9.** The $(\lambda - G_{RP})/(G_{BP} - G_{RP})$ TCDs using the stars selected from VPDs of clusters Czernik 14, Haffner 14, Haffner 17 and King 10. The continuous lines represent the slope determined through least-squares linear fit.

Kim et al. (2000) has specified the clusters tidal radius R_t as,

$$R_t = \left(\frac{M_c}{2M_G}\right)^{1/3} \times R_G$$

where R_t and M_c indicate the cluster's tidal radius and total mass (see Sect. 8), respectively. The estimated values of tidal radius are 9.71 ± 0.5 , 12.86 ± 0.7 , 13.11 ± 0.6 and 13.41 ± 0.5 pc for Czernik 14, Haffner 14, Haffner 17 and King 10, respectively and listed in Table 1.

4.3 Optical to mid-infrared extinction law

In this section, we combined multi-wavelength photometric data with Gaia astrometry to check the extinction law for clusters under study. The resultant $(\lambda - G_{RP})/(G_{BP} - G_{RP})$ two colour diagrams (TCDs) are shown in Fig 9 for all the clusters. Here, λ denotes the filters other than G_{RP} . All stars showing in Fig 9 are probable cluster members. A linear fit to the data points is performed and slopes are listed in Table 2. The estimated values of slopes are in good agreement with the value given by Shu Wang and Xiaodian Chen (2019). We estimated $\frac{A_V}{E(B-V)}$ as ~ 3.1 for all the clusters under study. This indicates that reddening law is normal towards the clusters under study.

4.4 Interstellar reddening from 2MASS colours

To estimate the cluster reddening in the near-IR region, we used $(J-H)$ versus $(J-K)$ colour-colour diagrams as shown in Fig 10. Stars plotted in this figure are the probable cluster members described in Sec. 3. The solid line is cluster's zero age main sequence (ZAMS) taken from Caldwell et al. (1993). The ZAMS shown by the dotted line is displaced by $E(J-H) = 0.30 \pm 0.03$ mag and $E(J-K) = 0.50 \pm 0.05$ mag for Czernik 14, 0.12 ± 0.04 and 0.25 ± 0.07 mag for Haffner 14, $E(J-H) = 0.40 \pm 0.05$ mag and $E(J-K) = 0.61 \pm 0.07$ mag for Haffner 17 and $E(J-H) = 0.34 \pm 0.04$ mag and $E(J-K) = 0.55 \pm 0.07$ mag for King 10. The solid line in this figure is theoretical isochrone taken from Marigo et al. (2017) of $\log(\text{age})=8.75, 8.50, 7.95$ and 7.65 for the clusters Czernik 14, Haffner 14, Haffner 17 and King 10, respectively. The ratio of $E(J-H)$ and $E(J-K)$ shows a good agreement with the normal value 0.55 proposed by Cardelli et al. (1989). Using $E(J-H)$ and $E(J-K)$, we have calculated the interstellar reddenings ($E(B-V)$) as, 0.96, 0.38, 1.29 and 1.09 for the clusters Czernik 14, Haffner 14, Haffner 17 and King 10, respectively. Our derived value of $E(B-V)$ is higher than Tadross (2014) for Czernik 14. The Present estimate of $E(B-V)$ is reliable than the value given by Tadross (2014) because it is based on the cluster members selected using proper motion data.

4.5 Age, distance and Galactocentric coordinates

The essential fundamental parameters (age, distance, and reddening) are estimated by fitting the solar metallicity ($Z = 0.019$) isochrones of Marigo et al. (2017) to all the CMDs ($G, G_{BP} - G_{RP}$), ($G, G_{BP} - G$), ($G, G - G_{RP}$), ($J, J - H$), ($J, J - W1$), ($J, J - W2$) & ($K, J - K$) as shown in Fig

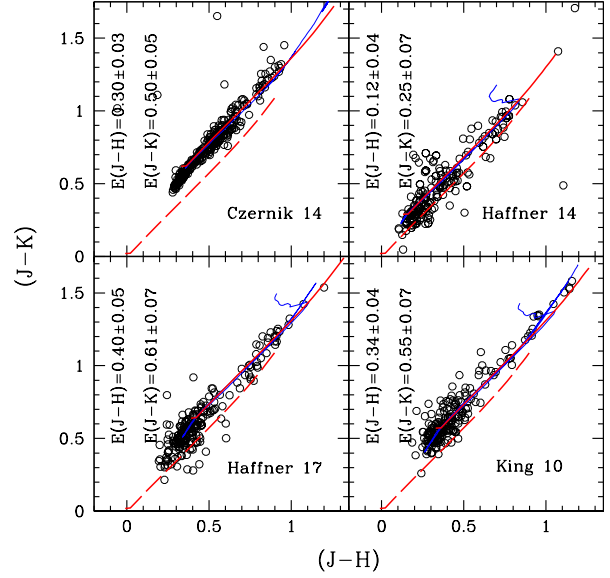


Figure 10. The colour-colour diagrams (CCDs) for clusters Czernik 14, Haffner 14, Haffner 17 and King 10 using probable cluster members. In CCDs, the red solid line is the ZAMS taken from Caldwell et al. (1993) while the red dotted lines are the same ZAMS shifted by the values as described in the text. The blue line is the theoretical isochrones of $\log(\text{age})=8.75, 8.50, 7.95$ and 7.65 for clusters Czernik 14, Haffner 14, Haffner 17 and King 10, respectively.

11 and Fig 12. To reduce the field star contamination we have used only probable cluster members based on clusters VPDs. The ratios $\frac{A_J}{A_V}=0.276$ and $\frac{A_H}{A_V}=0.176$ are taken from Schlegel et al. (1998), while the ratio $\frac{A_{K_s}}{A_V}=0.118$ was derived from Dutra et al. (2002). The Gaia DR2 absorption ratios $\frac{A_G}{A_V}=0.859$, $\frac{A_{G_{BP}}}{A_V}=1.068$ and $\frac{A_{G_{RP}}}{A_V}=0.652$ are taken from Henden (2018).

The galactocentric coordinates of the clusters X (directed towards the galactic center in the Galactic disc), Y (directed towards the Galactic rotation) and distance from the galactic plane Z (directed towards Galactic north pole) can be estimated using clusters' distances, longitude and latitude. The estimated Galactocentric coordinates are given in the corresponding paragraph of the clusters.

The estimation of the main fundamental parameters for the clusters are given below:

Czernik 14: We superimposed theoretical isochrones of different age ($\log(\text{age})=8.70, 8.75$ and 8.80) in all the CMDs for the cluster Czernik 14, shown in Fig 11. The overall fit is favorable for $\log(\text{age})=8.75$ (middle isochrone) to the brighter cluster members. The estimated apparent distance modulus $((m-M) = 15.10 \pm 0.2 \text{ mag})$ provides a distance 2.9 ± 0.20 kpc from the Sun. Present estimate of distance is very close to the value 3.0 kpc derived by Cantat-Gaudin (2018). The Galactocentric coordinates are derived as $X=2.32$ kpc, $Y=10.24$ kpc and $Z=0.04$ kpc. The Galactocentric distance of the cluster is calculated to be 10.49 ± 0.5 kpc. The value of Z indicates that Czernik 14 is

Table 2. Multi-band colour excess ratios in the direction of clusters Czernik 14, Haffner 14, Haffner 17 and King 10.

Band (λ)	Effective wavelength (nm)	Czernik 14	$\frac{\lambda - G_{RP}}{G_{BP} - G_{RP}}$ Haffner 14	Haffner 17	King 10
Johnson B	445	1.78 ± 0.02	1.50 ± 0.01	1.65 ± 0.02	1.82 ± 0.01
Johnson V	551	0.99 ± 0.01	0.88 ± 0.01	0.87 ± 0.02	0.95 ± 0.02
Pan-STARRS g	481	1.43 ± 0.02	1.33 ± 0.03	1.14 ± 0.03	1.42 ± 0.02
Pan-STARRS r	617	0.68 ± 0.03	0.60 ± 0.02	0.45 ± 0.03	0.69 ± 0.02
Pan-STARRS i	752	0.11 ± 0.03	0.06 ± 0.04	0.11 ± 0.04	0.13 ± 0.04
Pan-STARRS z	866	-0.20 ± 0.04	-0.21 ± 0.03	-0.26 ± 0.03	-0.19 ± 0.03
Pan-STARRS y	962	-0.37 ± 0.04	-0.32 ± 0.03	-0.41 ± 0.04	-0.36 ± 0.04
2MASS J	1234.5	-0.78 ± 0.03	-0.71 ± 0.04	-0.64 ± 0.03	-0.79 ± 0.04
2MASS H	1639.3	-1.20 ± 0.04	-1.12 ± 0.04	-1.07 ± 0.05	-1.24 ± 0.04
2MASS K	2175.7	-1.33 ± 0.06	-1.31 ± 0.07	-1.17 ± 0.06	-1.36 ± 0.05
WISE W1	3317.2	-1.38 ± 0.07	-1.27 ± 0.08	-1.21 ± 0.06	-1.41 ± 0.07
WISE W2	4550.1	-1.43 ± 0.08	-1.12 ± 0.09	-1.14 ± 0.07	-1.41 ± 0.08

above ~ 40 pc from Galactic plane.

Haffner 14: In the CMDs of Haffner 14, the isochrones of different age ($\log(\text{age})=8.45, 8.50$ and 8.55), are over plotted in Fig 11. A satisfactory fitting of isochrones provides an age of 320 ± 35 Myr for this object. The inferred apparent distance modulus ($m - M$) = 13.80 ± 0.3 mag provides a heliocentric distance as 4.8 ± 0.2 kpc. Our estimated value of distance is slightly higher than the value 3.9 kpc derived by Cantat-Gaudin (2018), but very close to the value derived by us using parallax. The Galactocentric distance is determined as 12.57 ± 0.9 kpc, which is calculated by considering 8.5 kpc as the distance of the Sun to the Galactic center. The Galactocentric coordinates are determined as $X=-3.05$ kpc, $Y=12.20$ kpc and $Z=-0.15$ kpc. This cluster is ~ 150 pc below the Galactic plane.

Haffner 17: Isochrones of different age ($\log(\text{age})=7.90, 7.95$ and 8.00) are used for the CMDs of Haffner 17, shown in Fig 12. By the isochrone fitting, we found an age 90 ± 10 Myr. The apparent distance modulus ($m - M$) = 16.20 ± 0.25 mag provides a heliocentric distance as 3.6 ± 0.1 kpc which is similar to 3.5 kpc derived by Cantat-Gaudin (2018). The Galactocentric distance is determined as 11.40 ± 0.7 kpc. The Galactocentric coordinates are determined as $X=-2.45$ kpc, $Y=11.13$ kpc and $Z=-0.14$ kpc. This cluster is ~ 140 pc below the Galactic plane.

King 10: We superimposed isochrones of different age ($\log(\text{age})=7.60, 7.65$ and 7.70) to CMDs, shown in Fig 12. This provides an age of 45 ± 5 Myr which is similar to the value 50 Myr derived by Mohan et al. (1992). The inferred apparent distance modulus ($m - M$) = 16.70 ± 0.3 mag provides a heliocentric distance as 3.8 ± 0.1 kpc which is not much different with 3.5 kpc derived by Cantat-Gaudin (2018). The Galactocentric distance is calculated as 9.76 ± 0.4 kpc. The Galactocentric coordinates are determined as $X=3.76$ kpc, $Y=9.10$ kpc and $Z=-0.02$ kpc. This cluster is very near to the Galactic plane.

4.5.1 Distance of clusters from Gaia DR2 parallax

Gaia DR2 has provided precise parallaxes for many stars in our sample clusters. Reliable value of distance can be estimated using the average value of parallax of cluster members

(Lauri et al. 2018). We have corrected Gaia DR2 parallax by adopting zero-point offset (-0.05 mas) as given by Riess et al. (2018). The histograms of parallax for the clusters in 0.15 mas bins are shown in Fig 13. In this figure, we also plotted G mag versus stars parallax. Black circles are all stars while blue denotes the probable cluster members. The dashed line indicates the average value of parallax for each cluster. The mean parallax is estimated as 0.30 ± 0.01 mas, 0.21 ± 0.02 mas, 0.28 ± 0.01 mas and 0.26 ± 0.01 mas for the clusters Czernik 14, Haffner 14, Haffner 17 and King 10 respectively and the corresponding distances are 2.9 ± 0.1 kpc, 4.8 ± 0.4 kpc, 3.6 ± 0.1 kpc and 3.8 ± 0.1 kpc. These values of cluster distance are in good agreement with the results obtained in the previous section.

5 DYNAMICS OF CLUSTERS

5.1 Luminosity and mass function

Generally, OCs represent hundreds of stars having similar ages and compositions but differ in masses. Luminosity and mass functions (LF&MF) mainly depends on the membership information of stars. The new data of Gaia DR2 are used to get reliable members using proper motions and parallaxes. The LF is the total number of member stars in different magnitude bins. To estimate the LF, we converted the apparent G magnitudes of main sequence stars into absolute one using the distance and reddening estimated in the present analysis. A histogram was constructed with 1.0-mag intervals and shown in Fig 14 for all the clusters under study. This figure shows that the LF continues to rise up to $M_G \sim 3.4, 3.4, 2.5$ and 2.0 mag for clusters Czernik 14, Haffner 14, Haffner 17 and King 10, respectively.

To transform the LF to MF, we used the theoretical isochrones of Marigo et al. (2017). Absolute magnitude bins are converted to mass bins. The resulting mass function created for the clusters is shown in Fig. 15. It can be described by a power-law given by,

$$\log \frac{dN}{dM} = -(1+x) \log(M) + \text{constant}$$

Where dN is the number of stars in a mass bin dM with central mass M and x is mass function slope. To

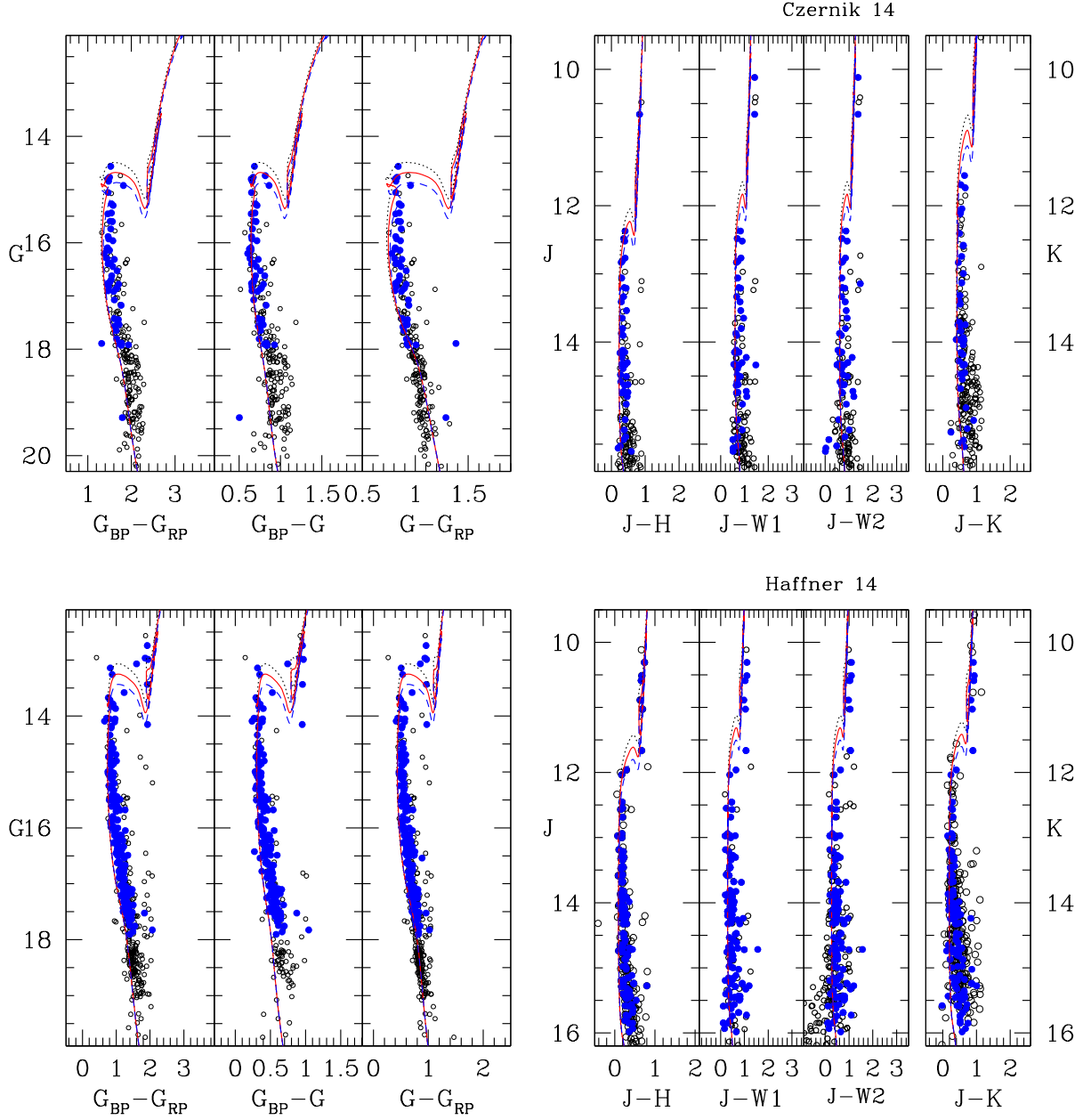


Figure 11. The G , $(G_{BP} - G_{RP})$, G , $(G_{BP} - G)$, G , $(G - G_{RP})$, J , $(J - H)$, J , $(J - W1)$, J , $(J - W2)$ and K , $(J - K)$ colour-magnitude diagrams of open star cluster Czernik 14 and Haffner 14. Black open circles are probable cluster members as selected from VPDs. Blue dots are most likely members with membership probability greater than 40 %. The curves are the isochrones of $(\log(\text{age})=8.70, 8.75 \text{ and } 8.80)$ for Czernik 14 and $(\log(\text{age})=8.45, 8.50 \text{ and } 8.55)$ for Haffner 14. All these isochrones are taken from Marigo et al. (2017) for solar metallicity.

derive the mass function, we only considered stars more massive than $1 M_{\odot}$ ($G \sim 19^{\text{th}}$ mag). This is because Gaia data (G mag) is not complete below $\sim 1 M_{\odot}$. (Arenou et al. (2018)). The initial mass function for massive stars ($\geq 1 M_{\odot}$) has been well studied and established by Salpeter (1955), where $x=1.35$. This form of Salpeter shows that the number of stars in each mass range decreases rapidly with the increasing mass. Our derived values of the MF slope, $x = 1.38 \pm 0.17, 1.27 \pm 0.10, 1.37 \pm 0.08$ and 1.29 ± 0.13 for

clusters Czernik 14, Haffner 14, Haffner 17 and King 10, respectively, are in good agreement with the Salpeters initial mass function slope within error. We have an estimated total mass of the clusters using the above mass function slope. The mass range, mass function slope and the total mass estimated in the present analysis are listed in the Table 3.

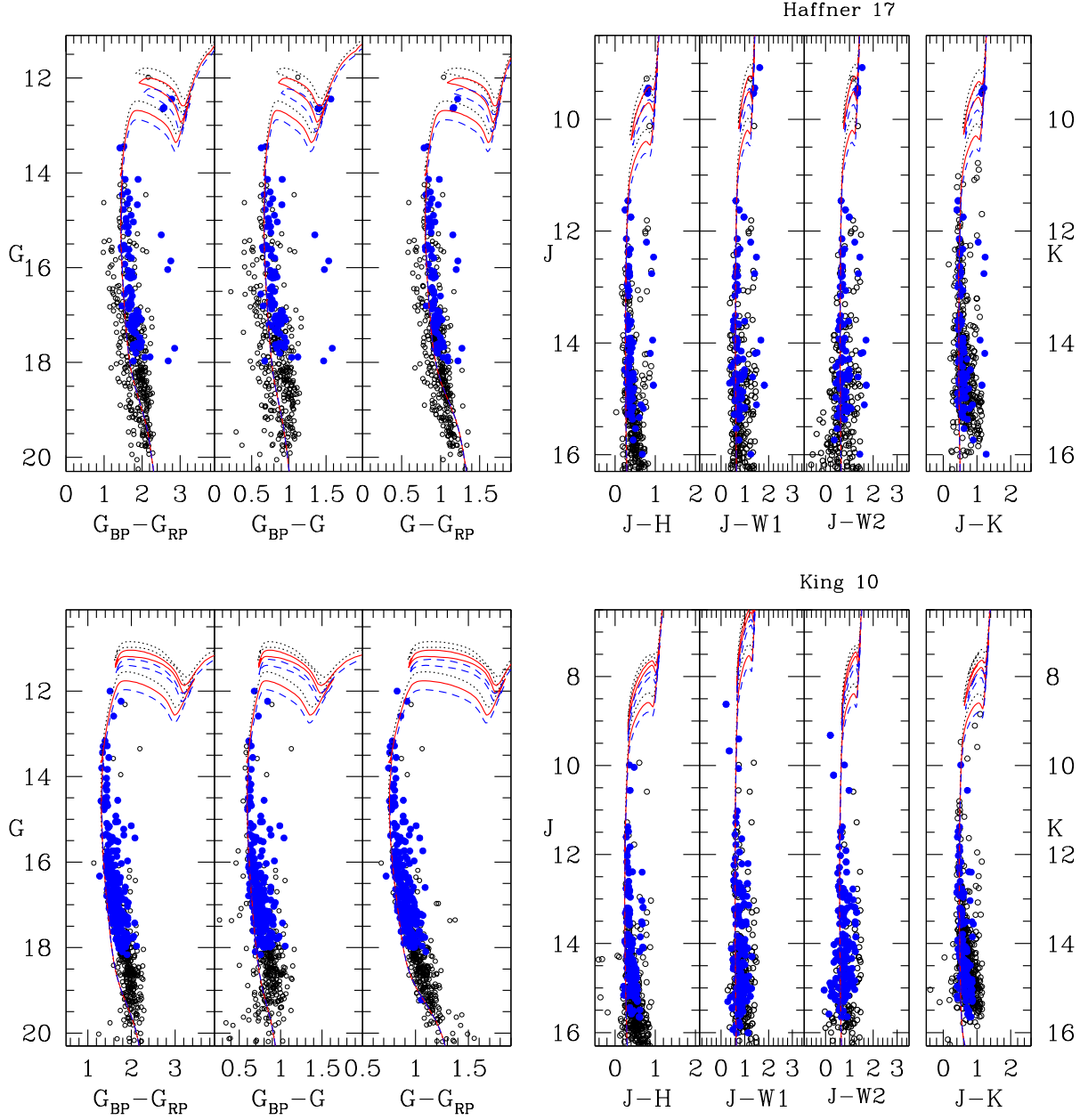


Figure 12. Same as Fig 11 for clusters Haffner 17 and King 10. The curves are the isochrones of ($\log(\text{age})=7.90, 7.95$ and 8.00) for Haffner 17 and ($\log(\text{age})=7.60, 7.65$ and 7.70) for King 10.

5.2 Mass-segregation

There are plenty of works related to mass-segregation of clusters in the literature (e.g. Sagar et al. 1988, Hillenbrand & Hartmann 1998, Lada & Lada 1991, Campbell et al. 1992, Pandey et al. 1992, Brandl et al. 1996, Meylan 2000, Bisht et al. 2019). Under this process, massive stars tend to move towards the core region and faint stars generally move towards the halo region of the cluster. For mass segregation study, we considered probable cluster members as selected in section 3. Cluster members are divided into three mass ranges as shown in Table 4 for the clusters under study.

We present cumulative radial stellar distribution of main sequence stars for three different mass ranges as shown in Fig 16. This diagram indicates that the cluster stars exhibit a mass-segregation in the sense that bright stars appear to be more centrally concentrated than the low mass members. We also performed the Kolmogorov-Smirnov test ($K-S$) to check the statistical significance of mass segregation. Using this test, we found the confidence level of mass-segregation as 91 %, 88 %, 75 % and 77 % for the clusters Czernik 14, Haffner 14, Haffner 17 and King 10 respectively.

The possible cause of the mass-segregation is not fixed and it changes from one cluster to another. The possible

Table 3. The main mass function parameters in clusters.

Object	Mass range	MF slope	Total mass	Mean mass
	M_{\odot}		M_{\odot}	M_{\odot}
Czernik 14	1.0 – 2.8	1.38 ± 0.17	348	1.55
Haffner 14	1.0 – 3.5	1.27 ± 0.10	595	1.68
Haffner 17	1.2 – 5.2	1.37 ± 0.08	763	2.18
King 10	1.4 – 7.2	1.29 ± 0.13	1088	2.75

Table 4. Distribution of stars in different mass ranges along with the percentage of confidence level in mass-segregation effect for the clusters.

Object	Mass ranges	Confidence level
	M_{\odot}	%
Czernik 14	3.8 – 2.2, 2.2 – 1.4, 1.4 – 1.0	91
Haffner 14	3.3 – 2.4, 2.4 – 1.3, 1.3 – 0.8	88
Haffner 17	5.2 – 3.7, 3.7 – 1.9, 1.9 – 1.2	75
King 10	7.2 – 4.7, 4.7 – 2.3, 2.3 – 1.4	77

reason for mass-segregation may be dynamical evolution or imprint of star formation or both in a particular cluster. Over the lifetime of clusters, encounters between its member stars gradually lead to an increased degree of energy equipartition throughout the clusters. The most important result of this process is that the bright stars gradually sink towards the cluster center and transfer their kinetic energy to the more numerous lower-mass stars, thus leading to mass segregation. To understand the reason for mass-segregation in the clusters, we calculated relaxation time (T_E). T_E is defined as the time in which the stellar velocity distribution becomes Maxwellian and expressed by the following formula:

$$T_E = \frac{8.9 \times 10^5 \sqrt{N} \times R_h^{3/2}}{\sqrt{m} \times \log(0.4N)}$$

where N is probable cluster members, R_h is the cluster half mass radius expressed in parsec and m is the average mass of the cluster members (Spitzer & Hart 1971) in the solar unit. We identified 225, 353, 350 and 395 stars as probable cluster members for Czernik 14, Haffner 14, Haffner 17 and King 10 respectively. The value of $\langle m \rangle$ is estimated as $1.55 M_{\odot}$, $1.68 M_{\odot}$, $2.18 M_{\odot}$ and $2.75 M_{\odot}$ for these clusters, respectively. The value of R_h is assumed to be equal to half of the cluster extent. Using the above formula of dynamical relaxation time, we estimated the value of T_E as 9.8, 20.4, 30, 27.2 Myr for Czernik 14, Haffner 14, Haffner 17 and King 10, respectively.

By using the cluster's age and dynamical relaxation time, we estimated the dynamical evolution parameter (τ) of the clusters using the following relation:

$$\tau = \frac{age}{T_E}$$

Our estimated values of relaxation time are found to be lower than the age of the clusters under study. This gives $\tau \geq 1.0$. Hence, we conclude that Czernik 14, Haffner 14, Haffner 17 and King 10 are dynamically relaxed open clusters.

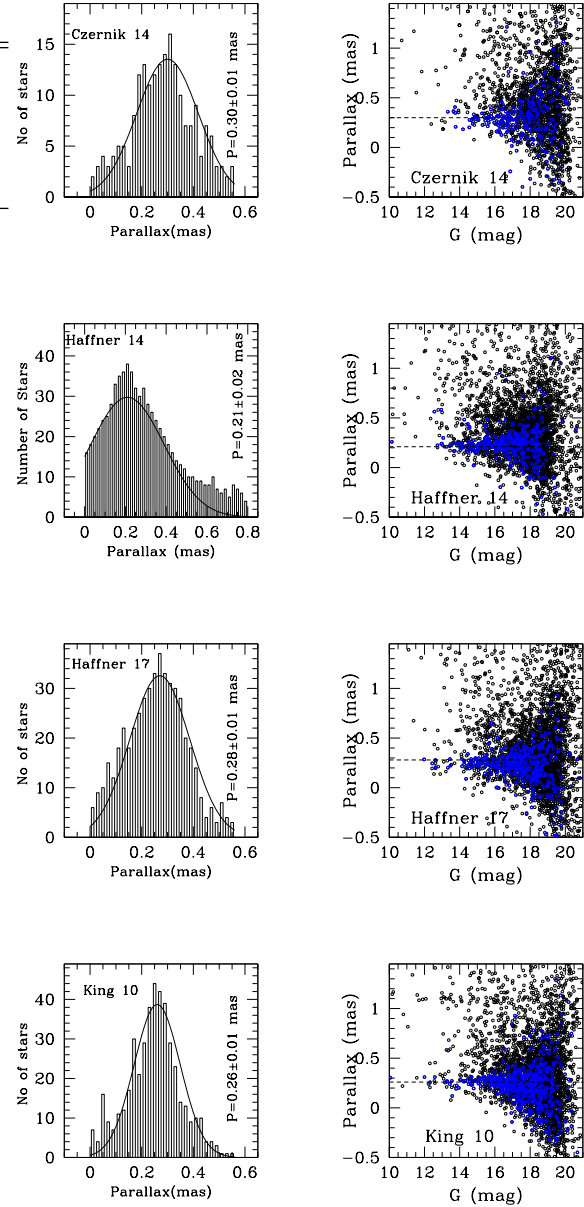


Figure 13. (left): Histogram for parallax estimation of the clusters Czernik 14, Haffner 14, Haffner 17 and King 10 using probable cluster members based on clusters VPDs. The Gaussian function is fitted to the central bins provides a mean value of parallax. (Right): G magnitude vs parallax diagrams. Black open circles are all stars while blue ones are probable cluster members. The dashed line is the mean value of clusters parallax.

6 ORBITS OF THE CLUSTERS

6.1 Galactic potential model

Galactic orbits are helpful to study the dynamical properties of stars, clusters and galaxies. We derived the Galactic orbits of the clusters under study using the Galactic potential models. We adopted the approach given by Allen & Santillan (1991) for Galactic potentials. According to

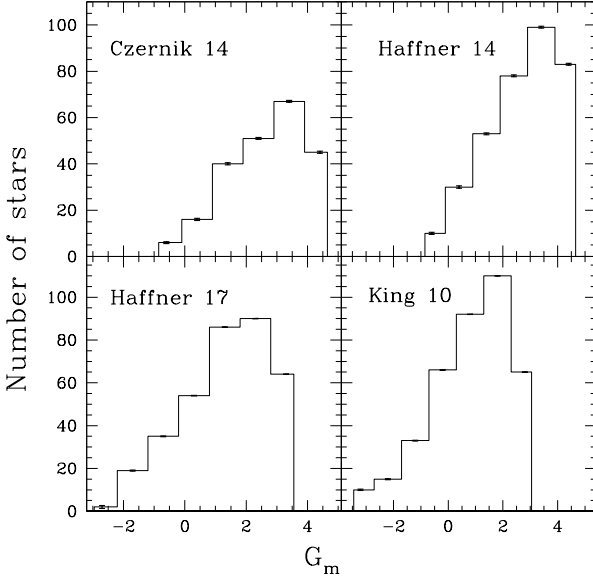


Figure 14. Luminosity function of main sequence stars in the region of the clusters Czernik 14, Haffner 14, Haffner 17 and King 10.

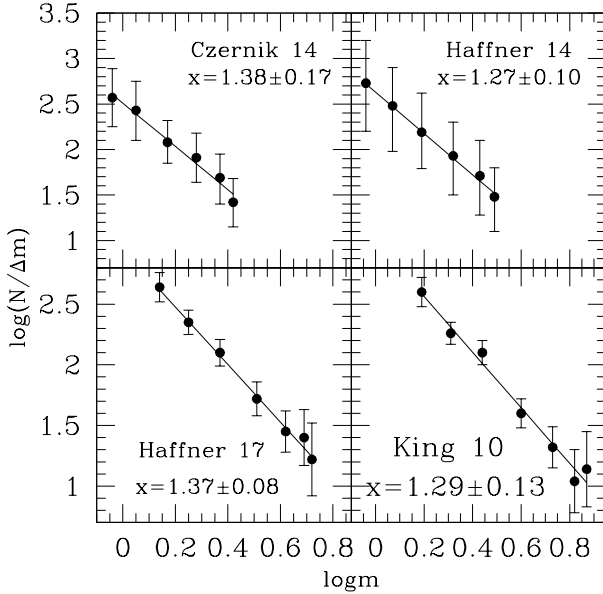


Figure 15. Mass function for the clusters Czernik 14, Haffner 14, Haffner 17 and King 10 derived using probable cluster members and Marigo et al. (2017) isochrones. The error bars represent $\frac{1}{\sqrt{N}}$.

their model, the mass of Galaxy is described by three components: spherical central bulge, massive spherical halo and disc. Recently Bajkova & Bobylev (2016) and Bobylev et. al (2017) refined the parameters of Galactic potential models with the help of new observational data

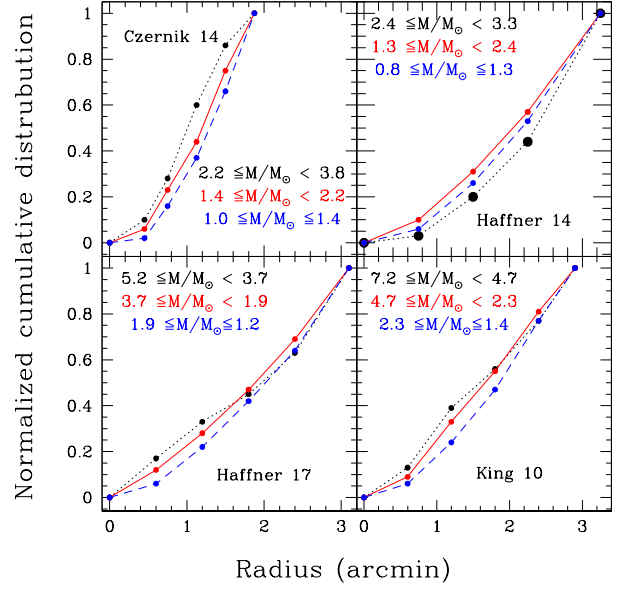


Figure 16. The cumulative radial distribution for Czernik 14, Haffner 14, Haffner 17 and King 10 in various mass-ranges.

for a distance $R \sim 0$ to 200 kpc. These potentials are given as

$$\begin{aligned}\Phi_b(r, z) &= -\frac{M_b}{\sqrt{r^2 + b_b^2}} \\ \Phi_d(r, z) &= -\frac{M_d}{\sqrt{r^2 + (a_d + \sqrt{z^2 + b_d^2})^2}} \\ \Phi_h(r, z) &= -\frac{M_h}{a_h} \ln\left(\frac{\sqrt{r^2 + a_h^2 + a_h}}{r}\right)\end{aligned}$$

Where Φ_b , Φ_d and Φ_h are the potentials of central bulge, disc and halo of Galaxy respectively. r and z are the distances of objects from Galactic center and Galactic disc respectively. The halo region potential is given by Wilkinson & Evans (1999). All three potentials are axis-symmetrical, time independent and analytical. Also, their spatial derivatives are continuous everywhere.

6.2 Orbits Calculation

The input parameters, such as central coordinates (α and δ), mean proper motions ($\mu_\alpha \cos \delta$, μ_δ), parallax angles, clusters age and heliocentric distances (d_\odot) for the clusters under study have been used from Table 5. Radial velocity data has been used from Gaia DR2 catalogue for all the clusters. Average radial velocities of the clusters are calculated by taking the mean for all probable cluster members. After five iterations, the average radial velocity of the clusters are found as -55.12 ± 1.04 , 71.21 ± 1.03 , 49.97 ± 2.09 and -44.35 ± 1.83 km/s for the clusters Czernik 14, Haffner 14, Haffner 17 and King 10, respectively. Our estimated value of radial velocities are in good agreement with Soubiran et al. (2018) for clusters Czernik 14 and Haffner 14. For clusters Haffner 17 and King 10, our estimated values are slightly higher than Soubiran et al. (2018). The Present estimate of radial velocity for Haffner 17 and King 10 is based on 24

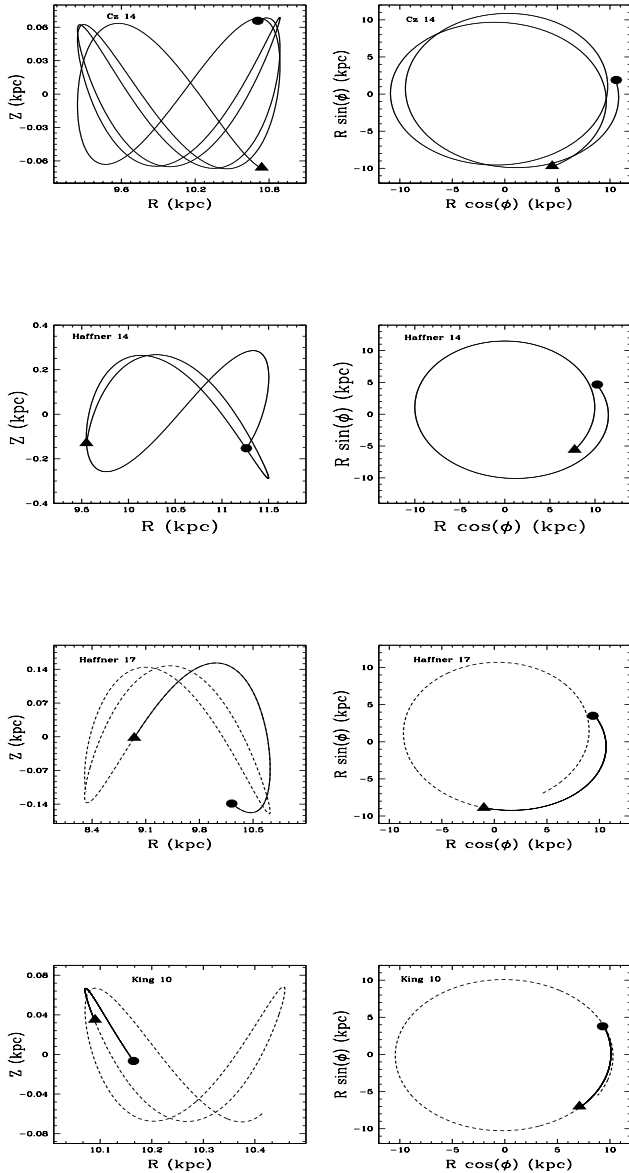


Figure 17. Galactic orbits of the clusters Czernik 14, Haffner 14, Haffner 17 and King 10 estimated with the Galactic potential model described in text in the time interval of the age of each cluster. For Haffner 17 and King 10, the dotted line represents cluster orbits for a time interval of 300 Myr. The left panel shows a side view and the right panel shows a top view of the cluster's orbit. The filled triangle and filled circle denotes birth and present day position of clusters in the Galaxy.

and 22 stars while in Soubiran et al. (2018) it is on 4 and 1 star respectively.

Since clusters are orbiting around the Galactic center, we cannot use position and velocity vectors in the equatorial system. Therefore, we transformed them, into the Galactocentric cylindrical coordinate system using the transformation matrix given in Johnson & Soderblom (1987). In this

system, (r, ϕ, z) indicates the position of an object in Galaxy, where r is the distance from Galactic center, ϕ is the angle relative to Sun's position in the Galactic plane and z is the distance from Galactic plane.

The right-hand coordinate system is adopted to transform equatorial velocity components into Galactic-space velocity components (U, V, W) , where U , V and W are radial, tangential and vertical velocities respectively. In this system the x-axis is taken positive towards Galactic-center, y-axis is along the direction of Galactic rotation and z-axis is towards Galactic north pole. The Galactic center is taken at $(17^h 45^m 32^s .224, -28^\circ 56' 10'')$ and North-Galactic pole is at $(12^h 51^m 26^s .282, 27^\circ 7' 42' .01)$ (Reid & Brunthaler, 2004). To apply a correction for Standard Solar Motion and Motion of the Local Standard of Rest (LSR), we used position coordinates of Sun as $(8.3, 0, 0.02)$ kpc and its space-velocity components as $(11.1, 12.24, 7.25)$ km/s (Schonrich et al. 2010). Transformed parameters in Galacto-centric coordinate system are listed in Table 6.

In orbit determination, we estimated the radial and vertical components of gravitational force, by differentiating total gravitational potentials with respect to r and z . The second order derivatives of gravitational force describe the motion of the clusters. For orbit determination, the second order derivatives are integrated backwards in time, which is equal to the age of clusters. Since potentials used are axis-symmetric, energy and z component of angular momentum are conserved throughout the orbits.

Fig. 17 show orbits of the clusters Czernik 14, Haffner 14, Haffner 17 and King 10. In left panels, the motion of clusters is described in terms of distance from Galactic center and Galactic plane, which shows two dimensional side view of the orbits. In right panels, cluster motion is described in terms of x and y components of Galactocentric distance, which shows a top view of orbits.

We also calculated the orbital parameters for the clusters and are listed in Table 7. Here e is eccentricity, R_a is apogalactic distance, R_p is the perigalactic distance, Z_{max} is the maximum distance travelled by cluster from Galactic disc, E is the average energy of orbits, J_z is z component of angular momentum and T is the time period of the clusters in the orbits.

The orbits of the clusters under study follow a boxy pattern and eccentricities for all the clusters are zero. Hence they trace a circular path around the Galactic center. From these orbits, we have determined the birth and present day position of clusters in the Galaxy which are represented by the filled circle and filled triangle respectively in Fig. 17.

Czernik 14 and Haffner 14 are intermediate age open star clusters while Haffner 17 and King 10 are younger objects with eccentricity ~ 0 . Orbits of these clusters are confined in a box of $9.0 < R_{gc} \leq 10.8$ kpc, $9.6 < R_{gc} < 11.6$ kpc, $8.2 < R_{gc} < 10.6$ kpc and $9.8 < R_{gc} < 10.5$ kpc for the clusters Czernik 14, Haffner 14, Haffner 17 and King 10, respectively. This indicates that all the clusters are outside the solar circle and not interacting within the inner region of the Galaxy. But all the clusters are orbiting near the Galactic disk, so they may be affected by the tidal forces of the disk which leads to a shorter life of the clusters. Carraro & Chiosi (1994) found that clusters which orbit in the outer region of the Galaxy can survive more as compared to the clusters which are in inner Galaxy. The similar result was

Table 5. Various fundamental parameters of the clusters Czernik 14, Haffner 14, Haffner 17 and King 10.

Parameter	Czernik 14	Haffner 14	Haffner 17	King 10
RA(deg)	49.25 ± 0.008	116.20 ± 0.004	117.90 ± 0.008	343.72 ± 0.005
DEC(deg)	58.59 ± 0.009	-28.37 ± 0.003	-31.81 ± 0.006	59.16 ± 0.007
Radius(arcmin)	3.5	3.7	6.2	5.7
Radius(parsec)	2.9	4.5	6.5	6.3
$\mu_{\alpha} \cos \delta (mas\ yr^{-1})$	-0.42 ± 0.02	-1.82 ± 0.009	-1.17 ± 0.007	-2.75 ± 0.008
$\mu_{\delta} (mas\ yr^{-1})$	-0.38 ± 0.01	1.73 ± 0.008	1.88 ± 0.006	-2.04 ± 0.006
Radial Velocity (Km/sec)	-55.12 ± 1.04	71.21 ± 1.03	49.97 ± 2.09	-44.35 ± 1.83
Age(My)	570 ± 60	320 ± 35	90 ± 10	45 ± 5
Metal abundance	0.019	0.019	0.019	0.019
E(J-H) (mag)	0.30 ± 0.03	0.12 ± 0.04	0.40 ± 0.05	0.34 ± 0.04
E(J-K) (mag)	0.50 ± 0.05	0.20 ± 0.07	0.61 ± 0.07	0.55 ± 0.07
E(B-V) (mag)	0.96 ± 0.05	0.38 ± 0.05	1.29 ± 0.05	1.09 ± 0.05
R_V	3.1	3.1	3.1	3.1
Distance modulus (mag)	15.10 ± 0.20	13.80 ± 0.10	15.10 ± 0.20	15.10 ± 0.20
Distance (Kpc)	2.90 ± 0.20	4.80 ± 0.20	3.6 ± 0.10	3.8 ± 0.10
X(Kpc)	2.32	-3.05	-2.45	3.76
Y(Kpc)	10.24	12.20	11.13	9.10
Z(Kpc)	0.04	-0.154	-0.14	-0.02
Total Luminosity(mag)	~ 3.4	~ 3.4	~ 2.5	~ 2.0
Cluster members	225	353	350	395
IMF slope	1.38 ± 0.17	1.27 ± 0.10	1.37 ± 0.08	1.29 ± 0.13
Total mass (M_{\odot})	~ 348	~ 595	~ 763	~ 1088
Average mass(M_{\odot})	1.55	1.68	2.18	2.75
Relaxation time(My)	9.8	20.4	30.3	27.2
Dynamical evolution parameter (τ)	~ 58	~ 16	~ 3	~ 1.6

Table 6. Position and velocity components in the Galactocentric coordinate system. Here R is the galactocentric distance, Z is the vertical distance from the Galactic disc, U V W are the radial tangential and the vertical components of velocity respectively and ϕ is the position angle relative to the sun's direction.

Cluster	R (kpc)	Z (kpc)	U (km/s)	V (km/s)	W (km/s)	ϕ (radian)
Czernik 14	10.71	0.07	16.16 ± 0.81	-229.41 ± 0.67	01.05 ± 0.29	0.17
Haffner 14	11.26	-0.15	19.16 ± 0.50	-226.74 ± 1.87	11.49 ± 0.09	0.39
Haffner 17	10.22	-0.14	32.57 ± 0.38	-226.07 ± 1.96	-04.27 ± 0.09	0.33
King 10	10.16	-0.01	-05.44 ± 1.04	-247.40 ± 1.79	04.04 ± 0.10	0.36

also found by Rangwal et. al (2019) for the cluster NGC 2506. Webb et al. (2014) found that clusters having circular orbits evolve slower as compared to the eccentric ones. The clusters in our sample have circular orbits and hence they evolve slowly. Orbital parameters determined in the present analysis are very much similar to the parameters found by Wu et al. (2009), except their orbits, are more eccentric than what we found in the present analysis.

7 CONCLUSIONS

In the present paper, we have investigated four poorly studied open clusters namely Czernik 14, Haffner 14, Haffner 17 and King 10 using the multi-colour photometric database along with Gaia DR2 astrometry. The reliable fundamental parameters have been estimated for these clusters and are listed in Table 5. Our main findings of the present analysis are following:

(i) The new center coordinates are estimated as ($\alpha^{\circ} = 3^h 17^m 00^s$, $\delta^{\circ} = 58^{\circ} 35' 24''$) for Czernik 14, ($\alpha^{\circ} = 7^h 44^m 48^s$,

$\delta^{\circ} = -28^{\circ} 22' 12''$) for Haffner 14, ($\alpha^{\circ} = 7^h 51^m 31^s$, $\delta^{\circ} = -31^{\circ} 49' 48''$) for Haffner 17 and ($\alpha^{\circ} = 22^h 54^m 53^s$, $\delta^{\circ} = 59^{\circ} 10' 12''$) for King 10.

(ii) Cluster extent is determined as 3.5 arcmin (2.9 parsec), 3.7 arcmin (4.5 parsec), 6.2 arcmin (6.5 parsec) and 5.7 arcmin (6.3 parsec) for Czernik 14, Haffner 14, Haffner 17 and King 10 respectively.

(iii) We have estimated the mean proper motion in both RA and DEC directions as (-0.42 ± 0.02 , -0.38 ± 0.01) $mas\ yr^{-1}$ for Czernik 14, (-1.82 ± 0.009 , 1.73 ± 0.008) $mas\ yr^{-1}$ for Haffner 14, (-1.17 ± 0.007 , 1.88 ± 0.006) $mas\ yr^{-1}$ for Haffner 17 and (-2.75 ± 0.008 , -2.04 ± 0.006) $mas\ yr^{-1}$ for King 10.

(iv) Colour-colour diagrams have been constructed after combining Gaia DR2, 2MASS, APASS, Pan-STARRS1 and WISE database. The diagrams indicate that interstellar extinction law is normal towards the cluster's region. Interstellar reddening ($E(B-V)$) have been determined as 0.96, 0.38, 1.29 and 1.09 mag for the clusters Czernik 14, Haffner 14, Haffner 17 and King 10 using 2MASS colours.

(v) Distances to the clusters Czernik 14, Haffner 14,

Table 7. Orbital parameters for the clusters obtained using the Galactic potential model.

Cluster	e	R_a (kpc)	R_p (kpc)	Z_{max} (kpc)	E (100km/s) ²	J_z (100 kpc km/s)	T (Myr)
Czernik 14	0.00	10.83	10.87	0.07	-09.84	-24.57	291
Haffner 14	0.00	11.50	11.50	0.29	-09.58	-25.54	310
Haffner 17	0.00	10.63	10.70	0.15	-10.15	-23.11	282
King 10	0.01	10.29	10.09	0.07	-09.73	-25.15	256

Haffner 17 and King 10 are determined as 2.9 ± 0.2 , 4.8 ± 0.2 kpc, 3.6 ± 0.1 kpc, and 3.8 ± 0.1 kpc respectively using CMDs. These distances are supported by the values estimated using mean parallax of the clusters. Ages of 570 ± 60 , 320 ± 35 , 90 ± 10 and 45 ± 5 Myr are determined for Czernik 14, Haffner 14, Haffner 17 and King 10 respectively by comparing with the theoretical isochrones of $Z=0.019$ taken from Marigo et al. (2017).

(vi) The LFs and MFs are determined by considering the members selected from Gaia proper motion database. The overall mass function slopes $x = 1.38 \pm 0.17$, 1.27 ± 0.10 , 1.37 ± 0.08 and 1.29 ± 0.13 are derived for Czernik 14, Haffner 14, Haffner 17 and King 10 respectively. The MF slopes are in good agreement with the Salpeter (1955) value for the clusters under study. Total mass was estimated as $\sim 348 M_\odot$, $\sim 595 M_\odot$, $\sim 763 M_\odot$ and $\sim 1088 M_\odot$ for clusters Czernik 14, Haffner 14, Haffner 17 and King 10 respectively.

(vii) Evidence of mass-segregation was observed for these clusters using probable cluster members. The K-S test shows the confidence level of mass-segregation as 91 %, 88 %, 75 % and 77 % for Czernik 14, Haffner 14, Haffner 17 and King 10 respectively. The cluster's age is higher than the relaxation time which indicates that all clusters are dynamically relaxed.

(viii) The mean radial velocities (-55.12 ± 1.04 km/s for Czernik 14, 71.21 ± 1.03 km/s for Haffner 14, 49.97 ± 2.09 km/s for Haffner 17 and -44.35 ± 1.83 km/s for King 10) are estimated from the Gaia DR2 database. Galactic orbits and orbital parameters are determined using Galactic potential models. We found that these objects are orbiting in a boxy pattern. The different orbital parameters are listed in Table 6 and 7 for the clusters under study.

ACKNOWLEDGEMENTS

This work has been financially supported by the Natural Science Foundation of China (NSFC-11590782, NSFC-11421303). This work has made use of data from the European Space Agency (ESA) mission Gaia (<https://www.cosmos.esa.int/gaia>), processed by the Gaia Data Processing and Analysis Consortium (DPAC, <https://www.cosmos.esa.int/web/gaia/dpac/consortium>).

Funding for the DPAC has been provided by national institutions, in particular the institutions participating in the Gaia Multilateral Agreement. In addition to this, It is worthy to mention that, this work has been done by using WEBDA and the data products from the Two Micron All Sky Survey (2MASS), which is a joint project of the University of Massachusetts and the Infrared Processing and Analysis Center/California Institute of Technology, funded by the National Aeronautics and Space Administration and the National Science Foundation (NASA).

REFERENCES

- Allen, C. & Martos, M. 1988, RMxAA, 16, 25
 Allen, C. & Santillan, A. 1991, Rev. Mexicana Astron. Astrofis., 22, 255
 Arenou, F., Luri, X., Babusiaux, C. et al. 2018, A&A, 616, A17
 Bajkova, A. T. & Bobylev, V. V. 2016, Astronomy Letters, 42, 9
 Bate, M. R., Bonnell, I. A. & Bromm, V. 2003, MNRAS, 339, 577
 Baume, G., Vázquez, R. A. & Carraro, G. 2004, MNRAS, 355, 475
 Becker, W. & Fenkart, R. 1971, A&AS, 4, 241
 Bisht, D., Yadav, R. K. S. & Durgapal, A. K. 2017, NewA, 52, 55B
 Bisht, D., Yadav, R. K. S., Ganesh, S., Durgapal, A. K., Rangwal, G. & Fynbo, J. P. U. 2019, MNRAS, 482, 1471B
 Bobylev, V. V., Bajkova, A. T. & Gromov, A. O. 2017, Astronomy Letters, 43, 4
 Bonatto, Ch. & Bica, E. 2003, A&A, 405, 525
 Bonatto, C., Bica, E. & Girardi, L. 2004, A&A, 415, 571
 Bonatto, C., Kerber, L., Bica, E. & Santiago, B. X. 2006, A&A, 446, 121
 Bonatto, C. & Bica, E. 2009, MNRAS, 397, 1915
 Brandl, B., et al. 1996, ApJ, 466, 254
 Bukowiecki, L., Maciejewski, G., Konorski, P. & Strobel, A., 2011, Acta Astron., 61, 231
 Cantat-Gaudin, T., Jordi, C., Vallenari, A., et al. 2018, A&A, 618A, 93C
 Caldwell, J. A. R., Cousins, A. W. J., Ahlers, C. C., van Wamelen, P. & Maritz, E. J. 1993, South Astronomical Observatory, Circ No. 15
 Campbell, B., et al. 1992, AJ, 104, 1721
 Cardelli, J. A., Clayton, G. C. & Mathis, J. S. 1989, ApJ, 345, 245
 Carpenter, J. M. 2001, ApJ, 121, 2851
 Carraro, G. & Chiosi, C. 1994, A&A, 287, 761
 Carraro, G., Ng, Y. K. & Portinari, L. 1998, MNRAS, 296, 1045
 Carraro G., Chiosi C., 1994, A&A, 288, 751
 Chambers, K. C., Magnier, E. A., Metcalfe, N., et al. 2016, arXiv:1612.05560v3
 Cunha, K., Frinchaboy, P. M., Souto, D., et al. 2013, ApJL, 777, L1
 Dias, W. S., Alessi, B. S., Moitinho, A., Lepine, J. R. D., 2002, A&A, 389, 871
 Dutra, C., Santiago, B. & Bica, E. 2002, A&A, 381, 219
 Durgapal, A. K. & Pandey, A. K. 2001, A&A, 375, 840
 Evans, D. W., Riello, M., De Angeli, F., et al. 2018, A&A, 616, A4
 Elmegreen, B. G. 2000, ApJ, 539, 342

- Frinchaboy, P. M. et al. 2013, *ApJ*, 777L, 1F
- Froeblich, D., Scholz, A. & Raftery, C. L. 2007, *MNRAS*, 374, 399
- Gaia Collaboration et al., 2016a, *A&A*, 595, A1
- Gaia Collaboration et al., 2016b, *A&A*, 595, A2
- Gaia Collaboration et al. 2018a, *A&A*, 616, A1
- Gaia Collaboration et al. 2018b, *A&A*, 616, A11
- Genzel, R. & Townes, C. H. 1987, *ARA&A*, 25, 377
- Geisler, L., Claria, J. J. & Minniti, D. 1997, *PASP*, 109, 799
- Gibbons S. L. J., Belokurov V., Evans N. W., 2014, *MNRAS*, 445, 3788
- Glushkova, E. V., Kuposov, S. E., Zolotukhin, I. Y., Beletsky, Y. V., Vlasov, A. D. & Leonova, S. I. 2010, *Astronomy Letters*, 36, 75
- Harris, W. E. & Pudritz, R. E. 1994, *ApJ*, 429, 177
- Henden, A., Munari, U. 2014, *Contrib. Astron. Obs. Skalnate Pleso*, 43, 518
- Heden, A., Templeton, M., Terrell, D., et al. 2016, *VizieR Online Data Catalog*, II/336
- Hendy, W. H. M. 2018, *NRIAG Journal of Astronomy and Geophysics*, 7, 180-186
- Hillenbrand L. A., Hartmann L. W., *ApJ*, 492, 540
- Hodapp, K. W., Kaiser, N., Aussel, H., et al. 2004, *AN*, 325, 636
- Janes, K. A. 1979, *ApJS*, 39, 135
- Johnson, D. R. H. & Soderblom, D. R. 1987, *AJ*, 93, 864
- Jordi, C., Gebran, M., Carrasco, J. M., et al. 2010, *A&A*, 523, A48
- King, I. 1962, *AJ*, 67, 471
- Kim, S. S., Figger, D. F., Lee, H. M. & Morris, M. 2000, *ApJ*, 545, 301
- Kuposov, S. E., Glushkova, E. V., Zolotukhin, I. Y. 2008, *A&A*, 486, 771
- Kronberger, M., Teutsch, P., Alessi, B, et al. 2006, *A&A*, 447, 921
- Lada C. J., Lada, E. A., 1991, in Jones K., ed., *ASP Conf. Ser.*, Vol. 13, The formation and evolution of star clusters, *Astron. Soc. Pac.*, San Francisco, p.3
- Larson, R. B. 1999. *Star formation*. In: Nakamoto, T. (Ed.), *Nobeyama Radio Observatory, Japan*, p. 336
- Lindgren, L., Hernandez, J., Bombrun, A, et al. 2018, *A&A*, 616, A2
- Lucas, P. W., Hoare, M. G., Longmore, A, et al. 2008, *MNRAS*, 391, 136
- Luri X., et al., 2018, *A&A*, 616, A9
- Maciejewski, G. & Niedzielski, A. 2007, *A&A*, 467, 1065
- Magnier, E. A., Schlafle, E., Finkbeiner, D., et al. 2013, *ApJS*, 205, 20
- Marigo, P. et al. 2017, *ApJ*, 835, 77
- Magrini, L., Sestito, P., Randich, S. & Galli, D. 2009, *A&A*, 494, 95
- McMillan, Paul J., 2017, *MNRAS*, 465, 76M
- Meylan, G., 2000, *Massive stellar clusters*, conference held in strasbourg, france. In: Lanon, A., Boily, C. (Eds.), *Astronomical Society of the pacific Conference Series*, p.215
- Minniti, D., Lucas, P. W., Emerson, J. P, et al. 2010, *NewA*, 15, 433
- Mohan, V., Pandey, A. K., Paliwal, D. C., Sagar, Ram., Mahra, H. S. 1992, *BASI*, 20, 303M
- Pandey, A.K., Mahra, H. S., Sagar, R, 1992, *Bulletin Astronom. Soci. India* 20, 287
- Pandey, A. K., Nilakshi, Ogura, K., Sagar, R. & Tarusawa, K. 2001, *A&A*, 374, 504
- Pedreras, Mario H., 2000, *RMxAA*, 36, 13P
- Peterson, C. J. & King, I. R. 1975, *AJ*, 80, 427
- Phelps, R. L. & Janes, K. A. 1993, *AJ*, 106, 1870
- Piatti, A. E., Bica, E., Santos, Jr., J. F. C. & Clariá, J. J. 2002, *A&A*, 387, 108P
- Piskunov, A. E., Belikov, A. N., Kharchenko, N. V. & Sagar, R. 2004, *MNRAS*, 349, 1449
- Prisinzano, L., Carraro, G., Piotto, G., Seleznev, A. F., Stetson, P. B. & Saviane, I. 2001, *A&A*, 369, 851
- Rangwal, G., Yadav, R. K. S., Durgapal, A., Bisht, D. & Nardiello, D. 2019, *MNRAS*, 490, 1383
- Reid M. J., Brunthaler A. 2004, *ApJ*, 616, 872
- Riess A. G., et al., 2018, *ApJ*, 861, 126
- Romanishim, W. & Angel, J. R. P. 1980, *ApJ*, 235, 992
- Sagar, R., Miakutin, V. I., Piskunov, A. E., Dluzhnevskaja, O. B., 1988. *MNRAS* 234, 831
- Sagar, R. & Griffiths, W. K. 1998, *MNRAS*, 299, 777
- Salpeter, E. E. 1955, *ApJ*, 121, 161
- Salaris, M., Weiss, A. & Percival, S. M. 2004, *A&A*, 414, 163
- Scalo, J. M. 1986, *Fund. Cosmic Phys*, 11, 1
- Scalo, J. M. 1998, *The stellar initial mass function*. In: Gilmore, G., Parry, I., Ryan, S. (Eds.) *ASP Conf*, 142, p.201
- Schonrich, Ralph., Binney, James., Dehnen, Walter. 2010, *MNRAS*, 403, 1829S
- Schlegel, D. J., Finkbeiner, D. P. & Davis, M. 1998, *ApJ*, 500, 525
- Schlafly, E. F., Finkbeiner, D. P., Juric, M., et al. 2012, *ApJ*, 756, 158
- Soubiran et al. 2018, *A&A*, 623C, 2S
- Spitzer, L. & Hart, M. 1971, *ApJ*, 164, 399
- Skrutskie, M. et al. 2006, *AJ*, 131, 1163
- Stubbs, C. W., Doherty, P., Cramer, C. et al. 2010, *ApJS*, 191, 376
- Sung, H. & Bessell, M. S. 2004, *AJ*, 127, 1014
- Tadross, A. L. 2014, *NRIAG Journal of Astronomy and Geophysics*, 3, 88
- Tonry, J. L., Stubbs, C. W., Lykke, K. R., et al. 2012, *ApJ*, 750, 99
- van den Bergh, S. 2006, *AJ*, 131, 1559
- Wilkinson, M. I. & Evans, N. W. 1999, *MNRAS*, 310, 645
- Wright, E. L., Eisenhardt, P. R. M., Mainzer, A. K., Ressler, M. E., Cutri, R. M., Jarrett, T., Kirkpatrick, J. D. & Padgett, D. 2010, *AJ*, 140, 1868
- Wang, Shu. & Chen, Xiaodian. 2019, Preprint, (arXiv:1904.04575v2)
- Wu, Z. Y., Zhou, X., Ma, J. & Du, C. H. 2009, *MNRAS*, 399, 2146
- Yadav, R. K. S. & Sagar, R. 2002, *MNRAS*, 337, 133
- Yadav, R. K. S. & Sagar, R. 2004, *MNRAS*, 349, 1481